

MIT Open Access Articles

Design principles of 3D epigenetic memory systems

The MIT Faculty has made this article openly available. **Please share** how this access benefits you. Your story matters.

Citation: Owen, Jeremy A., Osmanović, Dino and Mirny, Leonid. 2023. "Design principles of 3D epigenetic memory systems." *Science*, 382 (6672).

As Published: 10.1126/science.adg3053

Publisher: American Association for the Advancement of Science (AAAS)

Persistent URL: <https://hdl.handle.net/1721.1/153004>

Version: Author's final manuscript: final author's manuscript post peer review, without publisher's formatting or copy editing

Terms of use: Creative Commons Attribution-Noncommercial-Share Alike;An error occurred on the license name.



Title: Design principles of 3D epigenetic memory systems

Authors: Jeremy A. Owen¹†, Dino Osmanović², Leonid Mirny^{1*}

Affiliations:

¹Department of Physics, Massachusetts Institute of Technology; Cambridge, USA

²Department of Mechanical and Aeronautical Engineering, UCLA; Los Angeles, USA

†Present address: Department of Chemistry, Princeton University; Princeton, USA

*Corresponding author. Email: leonid@mit.edu

Abstract: Cells remember their identities, in part, using epigenetic marks—chemical modifications placed along the genome. How can mark patterns remain stable over cell generations despite their constant erosion by replication and other processes? We developed a theoretical model which reveals that 3D genome organization can stabilize epigenetic memory, as long as (1) there is a large density difference between chromatin compartments, (2) modifying “reader-writer” enzymes spread marks in 3D, and (3) the enzymes are limited in abundance relative to their histone substrates. Analogous to an associative memory that encodes memory in neuronal connectivity, mark patterns are encoded in a 3D network of chromosomal contacts. Our model provides a unified account of diverse observations, and reveals a key role of 3D genome organization in epigenetic memory.

One-Sentence Summary: The 3D folding of the genome can help cells remember their identities.

Main Text:

Remembering gene expression states—that is, which genes are “on” or “off”—is a striking
5 capability of living cells. It is well-established that this “epigenetic” memory can be stably encoded
in the abundances of freely-diffusing transcription factors (TFs) regulating each other’s synthesis
(1–3). But in eukaryotes, such as ourselves, in addition to TF-based memory, there is evidence that
memory can be held locally to the genes, in the chromatin (4–7). It has been suggested that a seat
of this chromatin-based epigenetic memory could be the chemical modifications (“marks”) of the
10 DNA-bound histones, which vary across the genome in patterns correlated with gene expression.
However, chromatin and its marks are subject to large disruptions through the cell cycle, and it is
not clear what is required to make stable memories out of mark patterns. Here, we identify three
qualitative elements that together are sufficient for stable epigenetic memory. Our minimal
theoretical model incorporating these elements unites a battery of classic observations ascribed to
15 epigenetic memory of heterochromatin, makes predictions that emerging experimental techniques
can test, and suggests a functional role for a hallmark of nuclear organization—its 3D
compartmentalization.

Heterochromatin—the transcriptionally-silent, denser nuclear compartment—is rich in
particular histone marks, especially the lysine trimethylations H3K9me3 and H3K27me3. These
20 marks are made by so-called “reader-writer” enzymes (8, 9) which can bind marked histones
allosterically, stimulating their marking activity on neighboring histones, effectively “spreading”
marks between neighbors. Marks can be retained locally when the replication fork passes (10, 11),
but they are (by necessity) diluted in the process by newly synthesized, unmarked histones. The
combination of these two features is highly suggestive of a stable memory system, in which local
25 mark spreading accurately restores mark patterns after their partial erasure at replication. However,

simple mathematical models (12, 13) of this mechanism reveal a basic instability—if mark spreading is strong enough to restore a partially erased pattern, marks also spread ectopically to the rest of the chromosome.

Recent experiments suggest that reader-writer enzymes may be able to spread histone marks “in 3D” (9, 14, 15), that is, between histones that are nearby in space because of how chromatin is folded, not just “in 1D” along the chromatin polymer. Since histone marks also contribute to the spatial compartmentalization of the genome, this raises the tantalizing possibility of a *bidirectional* coupling between the 3D folding of chromatin and the marks on the chromatin polymer (16–19). Could this help stabilize memory? Recent theoretical work (19–22) has explored some consequences of this putative coupling, but broadly, these works have trouble achieving a self-sustaining memory of mark patterns. An understanding of the qualitative conditions required for chromatin-based epigenetic memory is yet to emerge.

Model

In search of design principles for epigenetic memory, we introduce and study a simple biophysical model in which memory will be held autonomously in mark patterns. In many prior models, mark patterns are sustained by external reinforcement, for example by “nucleation sites” or “genomic bookmarks” (12, 13, 23) that recruit modifying enzymes, or by a static 3D contact structure (24). But a pattern determined by external influences is not itself a seat of memory, and so we exclude such elements from our model.

We model chromatin as a long polymer of 10^4 monomers confined within a sphere (Figure 1A). This could represent, in a coarse-grained manner, all the chromatin in the nucleus, or just a chromosomal region of 2 Mb (i.e., 10^4 nucleosomes). Monomers in the polymer can be in one of two states—A or B—with B monomers representing marked, heterochromatic regions and A monomers representing unmarked, euchromatic ones. To represent the “stickiness” of

heterochromatin (25–28), B monomers experience a short-range attraction (Figure S14) to one another of magnitude α , which leads B monomers to spatially segregate from the A monomers, forming a denser compartment.

To model the 3D spreading of marks (Figure 1B), we suppose that A monomers turn into B monomers at a rate Sn_B , where n_B is the number of neighboring B monomers within a 3D interaction radius r_c (1.5 times the diameter of a monomer), and S is the spreading rate. B monomers turn back into A monomers at a constant rate L , uniformly at all sites, representing in aggregate the loss of marked histones due to the activity of demodifying enzymes (e.g., demethylases), histone exchange, and replicative dilution (see below). Our core results will prove insensitive to precisely how the loss of marks is modeled (Figure S2).

To represent the cell cycle (Figure 1C), we run our model in two alternating phases. During “interphase”, we assume the chromatin is frozen in place while marks are spread and lost, reaching a steady state. By contrast, in “mitosis”, we assume marks remain unchanged while the chromatin polymer is compacted into a condensed state. Then, to establish a new interphase state, the polymer is allowed to expand subject to interactions between marked regions, naturally leading to compartmentalization (Materials and Methods). We call each round of polymer dynamics followed by mark dynamics one “cell generation”. Our assumptions about the dynamics in each phase reflect experimental observations. In interphase, the gross 3D organization of chromatin is quite stable (29), whereas some marks can turn over completely on a timescale of minutes to hours (30, 31)—a time over which chromatin loci may displace by just ~ 0.2 to 0.4 microns (32). In mitosis, by contrast, repressive marks appear to be stable (33, 34), even as chromatin undergoes dramatic changes. Several factors may account for this, including inhibition of modifying enzymes by mitotic phosphorylation of the H3 tail (35, 36), decreased accessibility of mitotic chromatin, and

the short duration of mitosis. Later, we will loosen the assumptions we make about the phases (Figure S3, S4).

An initial pattern of A/B monomer identities is set prior to the first interphase, and is allowed to evolve over one or many cell generations. If, at later times, the pattern resembles the initial pattern, *and would do so for several possible initial patterns*, then the system can be said to exhibit memory.

Results

Marks localize to dense regions providing stable memory for one cell generation

Over a single cell generation, we find there is an extremely good memory of mark patterns. The steady state of the mark dynamics reached in the “interphase” closely resembles the initial mark pattern used to fold the polymer (Figure 2A and 2B). The steady-state pattern can recover after large perturbations, such as a complete randomization of the pattern (every monomer is randomly set to A or B) (Figure 2A), or wholesale erasure of half of the pattern (Figure 2B). The reason for the recovery of the pattern is that spreading marks tend to localize to dense regions—the remaining marks spread in 3D and restore the marks in the spatially dense compartment that was formed by the originally marked regions. It is as if the mark pattern has been “memorized” in the 3D configuration of the polymer.

An analogy to epidemic spreading can help us understand the localization of marks to dense regions quantitatively. The mark dynamics of our model are identical to a Susceptible-Infected-Susceptible (SIS) epidemic model on a network (37). The monomers of our polymer are like individuals whose “social” contact network (Figure 2D) is defined by the polymer configuration and the marked state is like the infected state. The infection, like marks, spreads at a rate S and infected individuals recover (lose marks) at the rate L . A key parameter for epidemic spreading

dynamics is the average number of neighbors d of an individual (monomer). Roughly, there is an “epidemic threshold” $1/d$, such that if S/L is below $1/d$, the infection will die out.

Returning to our model with a dense and diffuse compartment, with average numbers of neighbors d_+ and d_- , respectively, this suggests that when S/L lies in the range:

$$\frac{1}{d_+} \leq \frac{S}{L} \leq \frac{1}{d_-}$$

there should be sharp localization of marks to the dense compartment, with very few marks in the diffuse compartment (see Supplementary Text for a more careful discussion). Intuitively, this condition says that the system must be above the “epidemic threshold” in the dense region, and below it in the diffuse region. Consistently, simulations (Figure 2C) show localization of marks in an even broader range of S/L . As the strength of self-attraction α increases, the difference in the densities grows (Figure 2C, inset), further broadening this range. The analogy to epidemic spreading shows quantitatively how the density difference between the compartments underlies the sharp localization of marks to the dense compartment, providing robust recovery of the initial mark pattern within one cell generation.

Memory is lost over multiple cell generations

However, over multiple generations (Figure 3), something starkly different happens. Sweeping through the parameter space of our model (Figure 3B), what we find is an unstable, all-or-none behavior. When S/L is greater than a critical value $\lambda_c(\alpha)$ (which depends on α), an initially marked region grows uncontrollably until it covers the whole polymer. When S/L is less than the critical value, marks are instead lost globally. In both cases, memory of the initial state is lost within a few generations. When there is strong self-attraction and S/L is fine-tuned to very near the critical value, memory lasts longer, but even then, there is a clear tendency to uncontrolled spread or global loss of marks. The same basic instability is apparent in the closely related model

of Sandholtz et al. (21), who found that fine-tuning of parameters was required to achieve just 5 generations of mark pattern memory. Taken together, 3D spread of marks, even when coupled with 3D genome folding through the self-attraction of marks, is not enough to provide lasting epigenetic memory.

5 ***Enzyme limitation stabilizes epigenetic memory***

But so far, we have neglected a key biological fact, often omitted in biophysical models of mark dynamics. Marks do not spread themselves—spreading requires the action of a reader-writer enzyme, which in the nucleus is likely to be *limited* relative to its histone substrates. Estimates of the abundances of the histone methyltransferases PRC2 and SETB1 (38–40), for example, suggest
10 that they are hundreds to thousands of times less abundant than nucleosomes, which number in the tens of millions. To account for the limitation of the reader-writer enzymes we introduce a Michaelis-Menten-type scheme (41, 42) where A-B pairs that are within the interaction radius act as the substrate (Figure 3F). We find that adding enzyme limitation to our model remarkably stabilizes the memory of the initial mark pattern (Figure 3D, E) for hundreds of cell generations,
15 and over a broad range of parameters.

The effect of enzyme limitation is to replace the spreading rate S by an effective spreading rate S_{eff} that depends on the number of A-B pairs N_{AB} (Supplementary Text):

$$S_{\text{eff}} = \begin{cases} S & \text{if } N_{AB} < E_T \\ \frac{SE_T}{N_{AB}} & \text{if } N_{AB} \geq E_T \end{cases},$$

where E_T is the total amount of enzyme. Intuitively, the enzyme sets a maximum global
20 modification rate—the “ V_{max} ” of the enzyme, which equals SE_T . Where before marks would spread uncontrollably across the whole polymer, now the total number of marks is set by the balance of V_{max} and L to be $N_B = SE_T/L$. This fixing of the number of marks is sufficient to yield a stable memory of the mark *pattern*, e.g., the position of a marked domain (Figure 3D, Figure

S1). Stability of the mark pattern is also seen when loss occurs purely by replicational dilution (modeled as random loss of half the marks) once every cell cycle period T_{div} instead of at a constant loss rate L (Figure S2). The stable memory is seen across a broad range of parameters, as long as self-attraction is strong enough (Figure 3E), and it works without external reinforcement or fine tuning, as required by other models.

Design principles and model phenomenology

To summarize our findings so far, we have found a memory system that depends on three key ingredients—all characteristic of heterochromatin: (i) strong self-attraction of marked regions, leading to nuclear compartmentalization and densification of marked regions; (ii) 3D spread of marks, and; (iii) limitation of the “reader-writer” enzyme, relative to its substrates. Together, we propose that the presence of these elements amounts to a basic design principle for epigenetic memory systems that exploit 3D genome structure for their function. Our results suggest that heterochromatin may be dense *not* to sterically exclude transcriptional machinery (heterochromatin is likely highly permeable to polymerase-size particles (43)), but rather as a way to maintain the memory of heterochromatin.

A rich observable phenomenology follows directly from these elements, providing strong support for our model, as well as many new predictions to be tested by emerging experimental modalities.

The number of marks scales linearly with the enzyme concentration

First and most basically, our model relates the abundance of a mark to the activity (S) and concentration (E_T) of a reader-writer enzyme that makes it—in particular, we find a broad regime in which the number of marks is *linear* in both these quantities: $N_B = SE_T/L$. This prediction is at least consistent with the measured effects of EZH2 inhibition (44) and activating mutations (45, 46) on H3K27me3 levels (Supplementary Text), although a definitive test of linearity will require

careful quantitation of both sides of the equation. Perhaps more surprisingly, our model reveals that sometimes changing the concentration of an enzyme is different than uniformly changing its activity. This could shed light on mechanistic puzzles, such as the question of how the oncogenic mutant H3K27M histone reduces H3K27me₃—does it sequester limited PRC2 (effectively reducing E_T) (47), or does it persistently reduce its activity (e.g., S) after transient contact (38)? Our model predicts that varying E_T should change the number of marks smoothly, whereas reducing S/L below a critical value can cause a sharp, global loss of marks (Figure S5).

Stable domains remain only partly marked

Second, our model predicts that only about half of monomers in marked regions are marked. As S/L or E_T is varied, the stable mark domains (Figure 3E) arising in the limited enzyme regime vary in length, but the fraction of monomers within the domain that are marked remains roughly constant, around 0.55 (Figure S6A). This “semimarking” phenomenon is consistent with several experimental results. Semimarking leads to a density difference of 2 to 3 fold between compartments (Figure S6B), consistent with observed differences between heterochromatic and euchromatic regions in the nucleus (48). Semimarked domains also fold into irregular structures (Figure S6B) as recently observed by superresolution microscopy targeting Polycomb-repressed *Hox* genes (49), instead of spheres as would fully marked domains. Additionally, semimarking explains the counterintuitive findings of Alabert et al. (50) that certain histone marks require several cell generations to be fully established on new histones after replicational dilution, and that old histones keep getting marked—our model naturally reproduces these observations (Figure S7).

Mark redistribution and error correction

Third, our model predicts a coupling between distant genomic regions, mediated by the titration of the limited enzyme. The plainest consequence of this is that if marks are lost somewhere, they tend to be gained elsewhere. In capturing this, our model agrees with the

numerous observations of such titration effects in epigenetic systems (51–53). As one illustration of this, we show that our model (Figure S8) can emulate the findings of Kraft et al. (15) that genomic deletion of PRC2 nucleation sites can cause loss of H3K27me3 local to the deletion but gain of the mark elsewhere.

5 We find that this “mark redistribution” has a natural directionality to it—marks tend to flow from smaller domains to larger domains. A pattern consisting of multiple, noncontiguous mark domains can be remembered for hundreds of generations (Figure 4A). However, we observe that over a longer timescale, the separate domains compete with one another for the limited enzyme (even when “infinitely” far apart, Figure S9), inexorably leading to the formation of a single big
10 domain.

The spontaneous formation of a big marked domain by mark redistribution after many cell generations is reminiscent of the formation of senescence-associated heterochromatin foci (SAHF) in senescent cells, which is associated with *loss* of heterochromatin elsewhere (54). Present accounts of SAHF formation suggest an orchestrated process regulated by many specific effectors
15 (55), but our findings highlight the possibility that similar behavior could be a primitive tendency of mark spreading coupled to 3D genome organization.

Longer domains are more stable against mark redistribution in direct proportion to their length (Figure S9). This effect extends to clusters of domains—as the inter-domain separation is decreased, they begin to act as a single larger domain, lasting longer in competition with a larger
20 domain (Figure 4B). These predictions could be tested by observing the fate of artificial ectopic mark domains of differing lengths (20, 56, 57), and clusters of small marked domains.

Since tiny domains are lost quickly, mark redistribution can be viewed as a form of error correction. If “errors” appear in the form of a background rate at which monomers spontaneously switch from A to B—creating “domains” consisting of individual monomers—these errors are

corrected immediately by redistribution of the marks to a larger domain (Figure 4C, Figure S10). Resistance to this kind of error is important for any model of epigenetic memory based on spreading by reader-writer enzymes, because these enzymes have (at some low, but nonzero rate) nonspecific “writing” activity, unstimulated by the “reader” domain (9). Conversely, this finding suggests that mechanisms other than ours must be at work in small, unusually stable mark domains, such as the three nucleosome *FLC* nucleation region of *Arabidopsis* (58, 59). Our model is compatible with such mechanisms—introducing small, permanently marked regions to our model does not alter the basic story (Figure S11).

Epigenetic heterogeneity can emerge stochastically and then remain stable

The final category of tests for our model stem from its ability to capture the emergence of epigenetic heterogeneity in a cell population. We consider the case in which marks are initially present in a small contiguous region and then S/L or E_T is suddenly increased (Figure 4D-I). This could represent a developmental event, such as an increase in the duration of the cell cycle (which effectively decreases L), or the overexpression/activation of a reader-writer enzyme (an increase in E_T). Immediately, new marks emerge randomly along the polymer, but over a few cell generations they redistribute to form one or a few large domains, strongly biased to include the small initially marked domain (Figure 4D, Movie S1). At the level of a population average (Figure 4E) the initial domain appears to simply expand *linearly* into a larger one. But in fact there is large single-cell variation involving noncontiguous domains (Figure 4F), a prediction single-cell epigenomic techniques (60) could test.

This behavior means that our model—without any modification or additional elements—can reproduce both classic and emerging aspects of the position-effect variegation (PEV). In PEV, translocations of the *white* gene of *Drosophila* to a genomic position near or within heterochromatin leads to stochastic, but mitotically-heritable, silencing of the gene (51). This

results in a “variegating” phenotype characterized by mottled red-white eyes, where clonal patches bear the same coloration. Thus, the state of the locus is stochastic yet memorized over many cell divisions. To see PEV in our model, we create cell lineage trees by simply duplicating our simulation after every generation, and then continuing the simulation of the copies independently.

5 We then interrogate the marking status of a small “regulatory region” somewhere along the polymer, to read out the silencing status over time in the lineage (Figure 4G-I). Solely by varying the position of this region, relative to the initially marked domain, our model reproduces strikingly different observed phenotypes—including both the “sectored” (Figure 4H) and “salt-and-pepper” (Figure 4I) modes of variegation (61, 62)—thus providing a mechanistic rationale for this classic

10 phenomenon of stochastically established yet memorized epigenetic states.

Discussion

To summarize, we have shown how three ingredients: self-attraction of marked regions, 3D spread of marks, and limited enzyme, give rise to stable mark patterns that could serve as seats of epigenetic memory. Of these ingredients, we want to especially highlight the importance of the

15 *limitation of reader-writer enzymes*—an element which is biologically very plausible, often neglected in models of mark dynamics, and which completely changes the system’s behavior.

The mechanism we identify accounts for the stable maintenance of mark domains after their establishment, but does not address the question of why certain regions get marked in the first place. Mark patterns can certainly be strongly influenced by processes we do not model here, such

20 as nucleation regions to which modifying enzymes are recruited (14, 23), or actively transcribed regions that are impervious to repressive marks (63–66). Our memory mechanism is compatible with such exogenous influences. Simulations in which we impose that some regions are “pinned” to be permanently marked (Figure S11) or conversely, are unmarkable (Figure S12), exhibit stable memory of mark domains away from pinned regions. It is also possible that some genomic

elements are required to “license” certain regions for memory (67, 68). Such “conditional nucleation sites” (20) could be modeled as markable regions separated by large unmarkable ones. In fact, in our model, this kind of architecture may help memory by slowing mark redistribution (Figure S12B).

5 Our model makes a number of assumptions and has several limitations, including its consideration of just a single epigenetic mark rather than competing or successive levels of modification, as well as the absence of heterochromatic attraction to the nuclear lamina. We explored variants of our model that relax two of our central assumptions: the absence of mitotic mark dynamics and the absence of interphase chromatin dynamics. We find that spreading of marks during mitosis has only a small effect, most fundamentally because mitosis is short in duration relative to the length of the cell cycle (Figure S3, Supplementary Text). This effect compounds (Figure S3B) with any reduced activity of modifying enzymes on mitotic chromatin (e.g., due to reduced chemical or physical accessibility), further diminishing the role of possible mitotic spread of marks. Interphase dynamics can accelerate the loss of mark patterns (especially when loss is solely due to replicative dilution), but we find this can be rescued by increasing the strength of self-attraction (Figure S4, Supplementary Text). Tethering of heterochromatin to the lamina might also play this role, hinting at a mechanism that could link disruptions of the lamina to epigenetic memory (69, 70).

20 A natural question about epigenetic memory systems is how much information can be stored, and for how long? As a first step towards addressing this question for our system, we chose a scheme for recording and reading out “bits” in a mark pattern, and then investigated how the probability of a bit error grows over successive cell generations in our model (Figure S13, Supplementary Text). We uncover a capacity-stability tradeoff—the more bits one seeks to encode (in our polymer of fixed length), the shorter the memory. For example, our system can reliably

memorize at least 8 bits for 50 generations, or at least 17 bits for 20 generations. These are only lower bounds on the capacity, as we have not shown that our scheme for encoding bits is optimal. Errors arise by mark redistribution, and we only poorly understand what controls the redistribution timescale, aside from the expectation that it will increase with system size. Despite these caveats, our estimate gives us a sense of scale—a mechanism like ours (using only 10^4 monomers), could provide stability to 250 ($\sim 2^8$) alternative cellular states over 50 generations.

Intuitively, the memory mechanism we uncover relies on the encoding of memory in different forms in different phases of the cell cycle. In interphase, memory is held in the 3D structure of the genome, in the form of density differences, because dynamic marks sharply localize to dense regions. During mitosis, when the 3D structure is being totally reorganized, memory is held in the 1D sequence of marks.

The mark dynamics on a fixed polymer in our model clearly has some affinity to the protein sequence design problem (71–73) where the goal is to find an amino acid sequence that will fold into a target 3D structure. Classically, the design may be accomplished by choosing a sequence that minimizes the energy of the target configuration relative to all other configurations (74, 75). Analogously, our mark dynamics—although not directly minimizing the energy of a target structure—nevertheless performs a kind of sequence design, giving rise to a mark sequence that refolds into a similar polymer structure. The dynamics of our model could then be thought of as iterated rounds of design and refolding, with the goal of preserving the sequence—a problem that is different from sequence design, and that to our knowledge has not been considered in the protein folding field.

The encoding of a mark pattern via folding of the polymer, within one cell generation, could also be thought of as the “learning rule” of an associative memory in a Hopfield network (76). Learning by the Hebb rule in such networks strengthens connections between active neurons

(77, 78)—here, connections between marked regions are established by folding them together (“*mark* together, *park* together”). In this analogy, the mark dynamics are like the “update rule” that allows recovery of a stored memory. This lens is particularly relevant with the growing recognition that single cells (79–81) and simple chemical systems (82, 83) are capable of remarkably complex behaviors and memory. The possibility that epigenetic systems are capable not just of memory but also of more sophisticated information processing, such as associative learning, should be kept in mind—it may be the key to understanding them in their full complexity.

Materials and Methods

To simulate our model, we used polychrom (84), a lab-developed wrapper of OpenMM (85) for the polymer dynamics, and EoN (Epidemics on Networks) (86) for the mark dynamics. Our simulated polymer consists of 10000 monomers connected by harmonic bonds with natural length $l = 1$. Monomers are of two types, A and B . Every pair of monomers (of types i and j) additionally interacts according to the following interparticle potential (following Falk et al. (27)):

$$U(r) = \begin{cases} 30 - 210r^{12} + 180r^{14} & \text{if } r < 1 \\ -\alpha_{ij}(b(c(r - r_0)^2 - 1)(r - r_0)^{12} + 1) & \text{if } 1 < r < 1.5 \\ 0 & \text{if } r > 1.5 \end{cases}$$

where $b = 1.744 \times 10^8$, $c = 13.714$, $r_0 = 1.25$, and $\alpha_{ij} = \alpha$ if $i = j = B$ and is zero otherwise. This potential (plotted in Figure S14) is repulsive for $r < 1$, and models short-ranged attraction between $r = 1$ and $r = 1.5$ as a smoothed square well of depth α_{ij} . The potential is continuous, has a continuous derivative, and exhibits good behavior in numerical simulations. Finally, our polymer is confined to a sphere with radius chosen so that the volume fraction occupied by monomers is 5%. This value may be compared to a rough estimate for the volume fraction of nucleosomes in the nucleus, e.g., $\sim (30 \text{ million} \times 500 \text{ nm}^3) / 300 \mu\text{m}^3 = 0.05$.

In our simulations, the polymer is initialized using the “grow_cubic” function of polychrom (84), which generates a compact, unknotted random walk on cubic lattice. It is then relaxed from this state using the variable timestep Langevin integrator of OpenMM (error tolerance = 0.0005). Note that our simulation is performed in the underdamped (ballistic) regime (frictionCoeff = 0.01 inverse OpenMM “picoseconds”), to enable use of the efficient variable timestep integrator. This does not change the equilibrium distribution of the monomer positions, from which we are interested in sampling. For all our simulations we relax the polymer for 1000 OpenMM “picoseconds”, which is long enough for the polymer to expand to fill the confining sphere and to develop compartmentalization according to the monomer identities. As a control we vary this relaxation time by a factor of 10 in either direction, and observe no significant differences in the time evolution of mark patterns (Figure S15).

For the mark dynamics, we generate a contact graph G from the relaxed polymer configuration, where the vertices of the graph are all the monomers, and there is an edge between two vertices if the distance between the associated monomers is less than the spreading radius, 1.5 (as a control, we show consequences of varying this value in Figure S16). We then simulate the dynamics of spreading and loss on this graph G using the fast_SIS (87) function of EoN, which performs an exact stochastic simulation of the Markovian SIS model on the graph G . Note that these mark dynamics are nonequilibrium (violating detailed balance).

The marks relax, according to their dynamics, towards an extremely long-lived metastable state from which we seek to sample (the true steady-state of these dynamics is always the absorbing state where there are no marks at all). The mark relaxation time we use in all our simulations is 200 divided by the loss rate L , which appears more than sufficient to reach the metastable state. We test this by varying the relaxation time in both directions, and see no appreciable changes (Figure S15).

In the case of limited enzyme, where there is an effective spreading rate dependent on the number of marks (see Supplementary Text), we update the spreading rate according to the evolving number of marks 200 times each cell generation.

5 **References and Notes**

1. M. Ptashne, A genetic switch: Gene control and phage. lambda (1986).
2. T. S. Gardner, C. R. Cantor, J. J. Collins, Construction of a genetic toggle switch in *Escherichia coli*. *Nature*. **403**, 339–342 (2000).
3. R. Zhu, J. M. del Rio-Salgado, J. Garcia-Ojalvo, M. B. Elowitz, Synthetic multistability in mammalian cells. *Science*. **375**, eabg9765 (2021).
4. I. B. Dodd, M. A. Micheelsen, K. Sneppen, G. Thon, Theoretical analysis of epigenetic cell memory by nucleosome modification. *Cell*. **129**, 813–822 (2007).
5. S. Berry, M. Hartley, T. S. G. Olsson, C. Dean, M. Howard, Local chromatin environment of a Polycomb target gene instructs its own epigenetic inheritance. *Elife*. **4**, e07205 (2015).
6. I. B. Dodd, K. Sneppen, "Modeling Bistable Chromatin States" in *Epigenetics and Systems Biology* (Elsevier, 2017), pp. 145–168.
7. R. Bonasio, S. Tu, D. Reinberg, Molecular signals of epigenetic states. *Science*. **330**, 612–616 (2010).
8. R. Margueron, N. Justin, K. Ohno, M. L. Sharpe, J. Son, W. J. Drury Iii, P. Voigt, S. R. Martin, W. R. Taylor, V. De Marco, Others, Role of the polycomb protein EED in the propagation of repressive histone marks. *Nature*. **461**, 762–767 (2009).
9. M. M. Müller, B. Fierz, L. Bittova, G. Liszczak, T. W. Muir, A two-state activation mechanism controls the histone methyltransferase Suv39h1. *Nat. Chem. Biol.* **12**, 188–193 (2016).
10. N. Reverón-Gómez, C. González-Aguilera, K. R. Stewart-Morgan, N. Petryk, V. Flury, S. Graziano, J. V. Johansen, J. S. Jakobsen, C. Alabert, A. Groth, Accurate recycling of

parental histones reproduces the histone modification landscape during DNA replication. *Mol. Cell.* **72**, 239–249 (2018).

- 5 11. T. M. Escobar, O. Oksuz, R. Saldaña-Meyer, N. Descostes, R. Bonasio, D. Reinberg, Active and repressed chromatin domains exhibit distinct nucleosome segregation during DNA replication. *Cell.* **179**, 953–963 (2019).
12. N. A. Hathaway, O. Bell, C. Hodges, E. L. Miller, D. S. Neel, G. R. Crabtree, Dynamics and memory of heterochromatin in living cells. *Cell.* **149**, 1447–1460 (2012).
13. C. Hodges, G. R. Crabtree, Dynamics of inherently bounded histone modification domains. *Proceedings of the National Academy of Sciences.* **109**, 13296–13301 (2012).
- 10 14. O. Oksuz, V. Narendra, C.-H. Lee, N. Descostes, G. LeRoy, R. Raviram, L. Blumenberg, K. Karch, P. P. Rocha, B. A. Garcia, Others, Capturing the onset of PRC2-mediated repressive domain formation. *Mol. Cell.* **70**, 1149–1162 (2018).
- 15 15. K. Kraft, K. E. Yost, S. Murphy, A. Magg, Y. Long, M. R. Corces, J. M. Granja, S. Mundlos, T. R. Cech, A. Boettiger, Others, Polycomb-mediated genome architecture enables long-range spreading of H3K27 methylation. *BioRxiv* (2020).
16. E. E. Dormidontova, A. Y. Grosberg, A. R. Khokhlov, Intramolecular phase separation of a copolymer chain with mobile primary structure. *Macromolecular Theory Simulations.* **1**, 375–385 (1992).
- 20 17. D. Michieletto, E. Orlandini, D. Marenduzzo, Polymer model with epigenetic recoloring reveals a pathway for the de novo establishment and 3D organization of chromatin domains. *Physical Review X.* **6**, 041047 (2016).
18. R. Cortini, M. Barbi, B. R. Caré, C. Lavelle, A. Lesne, J. Mozziconacci, J.-M. Victor, The physics of epigenetics. *Rev. Mod. Phys.* **88**, 025002 (2016).
- 25 19. D. Jost, C. Vaillant, Epigenomics in 3D: importance of long-range spreading and specific interactions in epigenomic maintenance. *Nucleic Acids Res.* **46**, 2252–2264 (2018).
20. F. Erdel, E. C. Greene, Generalized nucleation and looping model for epigenetic memory of histone modifications. *Proceedings of the National Academy of Sciences.* **113**, E4180–E4189 (2016).
- 30 21. S. H. Sandholtz, Q. MacPherson, A. J. Spakowitz, Physical modeling of the heritability and maintenance of epigenetic modifications. *Proceedings of the National Academy of Sciences.* **117**, 20423–20429 (2020).
22. M. Katava, G. Shi, D. Thirumalai, Chromatin dynamics controls epigenetic domain formation. *bioRxiv* (2021).
- 35 23. D. Michieletto, M. Chiang, D. Coli, A. Papantonis, E. Orlandini, P. R. Cook, D. Marenduzzo, Shaping epigenetic memory via genomic bookmarking. *Nucleic Acids Res.* **46**, 83–93 (2018).

24. A. Z. Abdulla, C. Vaillant, D. Jost, Painters in chromatin: a unified quantitative framework to systematically characterize epigenome regulation and memory. *Nucleic Acids Res.* **50**, 9083–9104 (2022).
- 5 25. H. Bauer, Structure and arrangement of salivary gland chromosomes in *Drosophila* species. *Proceedings of the National Academy of Sciences.* **22**, 216–222 (1936).
26. A. R. Strom, A. V. Emelyanov, M. Mir, D. V. Fyodorov, X. Darzacq, G. H. Karpen, Phase separation drives heterochromatin domain formation. *Nature.* **547**, 241–245 (2017).
- 10 27. A. G. Larson, D. Elnatan, M. M. Keenen, M. J. Trnka, J. B. Johnston, A. L. Burlingame, D. A. Agard, S. Redding, G. J. Narlikar, Liquid droplet formation by HP1 α suggests a role for phase separation in heterochromatin. *Nature.* **547**, 236–240 (2017).
28. M. Falk, Y. Feodorova, N. Naumova, M. Imakaev, B. R. Lajoie, H. Leonhardt, B. Joffe, J. Dekker, G. Fudenberg, I. Solovei, Others, Heterochromatin drives compartmentalization of inverted and conventional nuclei. *Nature.* **570**, 395–399 (2019).
- 15 29. H. Strickfaden, A. Zunhammer, S. van Koningsbruggen, D. Köhler, T. Cremer, 4D chromatin dynamics in cycling cells: Theodor Boveri’s hypotheses revisited. *Nucleus.* **1**, 284–297 (2010).
30. C. Kadoch, R. T. Williams, J. P. Calarco, E. L. Miller, C. M. Weber, S. M. G. Braun, J. L. Pulice, E. J. Chory, G. R. Crabtree, Dynamics of BAF-Polycomb complex opposition on heterochromatin in normal and oncogenic states. *Nat. Genet.* **49**, 213–222 (2017).
- 20 31. P. Dobrinić, A. T. Szczurek, R. J. Klose, PRC1 drives Polycomb-mediated gene repression by controlling transcription initiation and burst frequency. *Nat. Struct. Mol. Biol.* **28**, 811–824 (2021).
- 25 32. M. Gabriele, H. B. Brandão, S. Grosse-Holz, A. Jha, G. M. Dailey, C. Cattoglio, T.-H. S. Hsieh, L. Mirny, C. Zechner, A. S. Hansen, Dynamics of CTCF-and cohesin-mediated chromatin looping revealed by live-cell imaging. *Science.* **376**, 496–501 (2022).
33. K. Ito, K. S. Zaret, Maintaining transcriptional specificity through mitosis. *Annu. Rev. Genomics Hum. Genet.* **23**, 53–71 (2022).
34. Y. Liu, B. Pelham-Webb, D. C. Di Giammartino, J. Li, D. Kim, K. Kita, N. Saiz, V. Garg, A. Doane, P. Giannakakou, A.-K. Hadjantonakis, O. Elemento, E. Apostolou, Widespread

mitotic bookmarking by histone marks and transcription factors in pluripotent stem cells.
Cell Rep. **19**, 1283–1293 (2017).

- 5 35. S. Rea, F. Eisenhaber, D. O’Carroll, B. D. Strahl, Z. W. Sun, M. Schmid, S. Opravil, K. Mechtler, C. P. Ponting, C. D. Allis, T. Jenuwein, Regulation of chromatin structure by site-specific histone H3 methyltransferases. *Nature*. **406**, 593–599 (2000).
36. P. N. I. Lau, P. Cheung, Histone code pathway involving H3 S28 phosphorylation and K27 acetylation activates transcription and antagonizes polycomb silencing. *Proc. Natl. Acad. Sci. U. S. A.* **108**, 2801–2806 (2011).
- 10 37. R. Pastor-Satorras, C. Castellano, P. Van Mieghem, A. Vespignani, Epidemic processes in complex networks. *Rev. Mod. Phys.* **87**, 925 (2015).
38. J. M. Stafford, C.-H. Lee, P. Voigt, N. Descostes, R. Saldaña-Meyer, J.-R. Yu, G. Leroy, O. Oksuz, J. R. Chapman, F. Suarez, Others, Multiple modes of PRC2 inhibition elicit global chromatin alterations in H3K27M pediatric glioma. *Science advances*. **4**, eaau5935 (2018).
- 15 39. R. Leicher, J. G. Eva, X. Lin, M. J. Reynolds, W. Xie, T. Walz, B. Zhang, T. W. Muir, S. Liu, Single-molecule and in silico dissection of the interaction between Polycomb repressive complex 2 and chromatin. *Proceedings of the National Academy of Sciences*. **117**, 30465–30475 (2020).
- 20 40. M. A. Gillespie, C. G. Pali, D. Sanchez-Taltavull, P. Shannon, W. J. R. Longabaugh, D. J. Downes, K. Sivaraman, H. M. Espinoza, J. R. Hughes, N. D. Price, T. J. Perkins, J. A. Ranish, M. Brand, Absolute Quantification of Transcription Factors Reveals Principles of Gene Regulation in Erythropoiesis. *Mol. Cell*. **78**, 960-974.e11 (2020).
41. K. A. Johnson, R. S. Goody, The original Michaelis constant: translation of the 1913 Michaelis--Menten paper. *Biochemistry*. **50**, 8264–8269 (2011).
- 25 42. J. Gunawardena, Time-scale separation--Michaelis and Menten’s old idea, still bearing fruit. *FEBS J.* **281**, 473–488 (2014).
43. A. Bancaud, S. Huet, N. Daigle, J. Mozziconacci, J. Beaudouin, J. Ellenberg, Molecular crowding affects diffusion and binding of nuclear proteins in heterochromatin and reveals the fractal organization of chromatin. *EMBO J.* **28**, 3785–3798 (2009).
- 30 44. M. T. McCabe, H. M. Ott, G. Ganji, S. Korenchuk, C. Thompson, G. S. Van Aller, Y. Liu, A. P. Graves, A. Della Pietra 3rd, E. Diaz, L. V. LaFrance, M. Mellinger, C. Duquenne, X. Tian, R. G. Kruger, C. F. McHugh, M. Brandt, W. H. Miller, D. Dhanak, S. K. Verma, P. J. Tummino, C. L. Creasy, EZH2 inhibition as a therapeutic strategy for lymphoma with EZH2-activating mutations. *Nature*. **492**, 108–112 (2012).
- 35 45. W. Béguelin, M. Teater, C. Meydan, K. B. Hoehn, J. M. Phillip, A. A. Soshnev, L. Venturutti, M. A. Rivas, M. T. Calvo-Fernández, J. Gutierrez, J. M. Camarillo, K. Takata, K. Tarte, N. L. Kelleher, C. Steidl, C. E. Mason, O. Elemento, C. D. Allis, S. H. Kleinstejn, A.

M. Melnick, Mutant EZH2 induces a pre-malignant lymphoma niche by reprogramming the immune response. *Cancer Cell*. **37**, 655-673.e11 (2020).

46. G. P. Souroullas, W. R. Jeck, J. S. Parker, J. M. Simon, J.-Y. Liu, J. Paulk, J. Xiong, K. S. Clark, Y. Fedoriw, J. Qi, C. E. Burd, J. E. Bradner, N. E. Sharpless, An oncogenic Ezh2 mutation induces tumors through global redistribution of histone 3 lysine 27 trimethylation. *Nat. Med.* **22**, 632–640 (2016).
47. K. L. Diehl, E. J. Ge, D. N. Weinberg, K. S. Jani, C. D. Allis, T. W. Muir, PRC2 engages a bivalent H3K27M-H3K27me3 dinucleosome inhibitor. *Proc. Natl. Acad. Sci. U. S. A.* **116**, 22152–22157 (2019).
48. H. D. Ou, S. Phan, T. J. Deerinck, A. Thor, M. H. Ellisman, C. C. O’shea, ChromEMT: Visualizing 3D chromatin structure and compaction in interphase and mitotic cells. *Science*. **357**, eaag0025 (2017).
49. S. Murphy, A. N. Boettiger, Polycomb repression of Hox genes involves spatial feedback but not domain compaction or demixing. *bioRxiv* (2022), p. 2022.10.14.512199, , doi:10.1101/2022.10.14.512199.
50. C. Alabert, T. K. Barth, N. Reverón-Gómez, S. Sidoli, A. Schmidt, O. N. Jensen, A. Imhof, A. Groth, Two distinct modes for propagation of histone PTMs across the cell cycle. *Genes Dev.* **29**, 585–590 (2015).
51. S. C. R. Elgin, G. Reuter, Position-effect variegation, heterochromatin formation, and gene silencing in Drosophila. *Cold Spring Harb. Perspect. Biol.* **5**, a017780 (2013).
52. C. M. Weber, A. Hafner, J. G. Kirkland, S. M. G. Braun, B. Z. Stanton, A. N. Boettiger, G. R. Crabtree, mSWI/SNF promotes Polycomb repression both directly and through genome-wide redistribution. *Nat. Struct. Mol. Biol.* **28**, 501–511 (2021).
53. E. Conway, F. Rossi, D. Fernandez-Perez, E. Ponzio, K. J. Ferrari, M. Zanotti, D. Manganaro, S. Rodighiero, S. Tamburri, D. Pasini, BAP1 enhances Polycomb repression by counteracting widespread H2AK119ub1 deposition and chromatin condensation. *Mol. Cell.* **81**, 3526-3541.e8 (2021).
54. X. Zhang, X. Liu, Z. Du, L. Wei, H. Fang, Q. Dong, J. Niu, Y. Li, J. Gao, M. Q. Zhang, W. Xie, X. Wang, The loss of heterochromatin is associated with multiscale three-dimensional genome reorganization and aberrant transcription during cellular senescence. *Genome Res.* **31**, 1121–1135 (2021).
55. I. Olan, M. Narita, Senescence: An Identity Crisis Originating from Deep Within the Nucleus. *Annu. Rev. Cell Dev. Biol.* **38**, 219–239 (2022).
56. P. I. Thakore, A. M. D’ippolito, L. Song, A. Safi, N. K. Shivakumar, A. M. Kabadi, T. E. Reddy, G. E. Crawford, C. A. Gersbach, Highly specific epigenome editing by CRISPR-

Cas9 repressors for silencing of distal regulatory elements. *Nat. Methods*. **12**, 1143–1149 (2015).

57. J. Pulecio, N. Verma, E. Mejía-Ramírez, D. Huangfu, A. Raya, CRISPR/Cas9-based engineering of the epigenome. *Cell Stem Cell*. **21**, 431–447 (2017).
- 5 58. H. Yang, S. Berry, T. S. G. Olsson, M. Hartley, M. Howard, C. Dean, Distinct phases of Polycomb silencing to hold epigenetic memory of cold in Arabidopsis. *Science*. **357**, 1142–1145 (2017).
59. C. Lövkvist, P. Mikulski, S. Reeck, M. Hartley, C. Dean, M. Howard, Hybrid protein assembly-histone modification mechanism for PRC2-based epigenetic switching and memory. *Elife*. **10** (2021).
- 10 60. S. Preissl, K. J. Gaulton, B. Ren, Characterizing cis-regulatory elements using single-cell epigenomics. *Nat. Rev. Genet.*, 1–23 (2022).
61. B. Y. Lu, C. P. Bishop, J. C. Eissenberg, Developmental timing and tissue specificity of heterochromatin-mediated silencing. *EMBO J*. **15**, 1323–1332 (1996).
- 15 62. F. Bughio, G. R. Huckell, K. A. Maggert, Monitoring of switches in heterochromatin-induced silencing shows incomplete establishment and developmental instabilities. *Proc. Natl. Acad. Sci. U. S. A.* **116**, 20043–20053 (2019).
63. F. W. Schmitges, A. B. Prusty, M. Faty, A. Stützer, G. M. Lingaraju, J. Aiwazian, R. Sack, D. Hess, L. Li, S. Zhou, R. D. Bunker, U. Wirth, T. Bouwmeester, A. Bauer, N. Ly-Hartig, K. Zhao, H. Chan, J. Gu, H. Gut, W. Fischle, J. Müller, N. H. Thomä, Histone methylation by PRC2 is inhibited by active chromatin marks. *Mol. Cell*. **42**, 330–341 (2011).
- 20 64. S. Henikoff, A. Shilatifard, Histone modification: cause or cog? *Trends Genet*. **27**, 389–396 (2011).
65. S. Berry, C. Dean, M. Howard, Slow chromatin dynamics allow polycomb target genes to filter fluctuations in transcription factor activity. *Cell systems*. **4**, 445–457 (2017).
- 25 66. C. Lövkvist, M. Howard, Using computational modelling to reveal mechanisms of epigenetic Polycomb control. *Biochem. Soc. Trans.* **49**, 71–77 (2021).
67. R. T. Coleman, G. Struhl, Causal role for inheritance of H3K27me3 in maintaining the OFF state of a Drosophila HOX gene. *Science*. **356** (2017), doi:10.1126/science.aai8236.
- 30 68. T. A. Shafiq, D. Moazed, Three rules for epigenetic inheritance of human Polycomb silencing. *bioRxiv* (2023), p. 2023.02.27.530239, , doi:10.1101/2023.02.27.530239.
69. D. K. Shumaker, T. Dechat, A. Kohlmaier, S. A. Adam, M. R. Bozovsky, M. R. Erdos, M. Eriksson, A. E. Goldman, S. Khuon, F. S. Collins, T. Jenuwein, R. D. Goldman, Mutant

nuclear lamin A leads to progressive alterations of epigenetic control in premature aging. *Proc. Natl. Acad. Sci. U. S. A.* **103**, 8703–8708 (2006).

70. A. Karoutas, A. Akhtar, Functional mechanisms and abnormalities of the nuclear lamina. *Nat. Cell Biol.* **23**, 116–126 (2021).
- 5 71. V. S. Pande, A. Y. Grosberg, T. Tanaka, Heteropolymer freezing and design: Towards physical models of protein folding. *Rev. Mod. Phys.* **72**, 259–314 (2000).
72. A. Y. Grosberg, A. R. Khokhlov, *Giant molecules: Here, there, and everywhere (2nd edition)* (World Scientific Publishing, Singapore, Singapore, 2010).
- 10 73. T. M. Fink, R. C. Ball, How many conformations can a protein remember? *Phys. Rev. Lett.* **87**, 198103 (2001).
74. E. I. Shakhnovich, A. M. Gutin, Engineering of stable and fast-folding sequences of model proteins. *Proc. Natl. Acad. Sci. U. S. A.* **90**, 7195–7199 (1993).
75. V. S. Pande, A. Y. Grosberg, T. Tanaka, Thermodynamic procedure to synthesize heteropolymers that can renature to recognize a given target molecule. *Proc. Natl. Acad. Sci. U. S. A.* **91**, 12976–12979 (1994).
- 15 76. J. J. Hopfield, Neural networks and physical systems with emergent collective computational abilities. *Proceedings of the national academy of sciences.* **79**, 2554–2558 (1982).
77. D. O. Hebb, *The Organization of Behavior*, McGill University (1949).
78. S. Löwel, W. Singer, Selection of intrinsic horizontal connections in the visual cortex by correlated neuronal activity. *Science.* **255**, 209–212 (1992).
- 20 79. J. P. Dexter, S. Prabakaran, J. Gunawardena, A complex hierarchy of avoidance behaviors in a single-cell eukaryote. *Curr. Biol.* **29**, 4323–4329 (2019).
80. S. J. Gershman, P. E. M. Balbi, C. R. Gallistel, J. Gunawardena, Reconsidering the evidence for learning in single cells. *Elife.* **10**, e61907 (2021).
- 25 81. M. Kramar, K. Alim, Encoding memory in tube diameter hierarchy of living flow network. *Proc. Natl. Acad. Sci. U. S. A.* **118** (2021), doi:10.1073/pnas.2007815118.
82. A. Murugan, Z. Zeravcic, M. P. Brenner, S. Leibler, Multifarious assembly mixtures: Systems allowing retrieval of diverse stored structures. *Proceedings of the National Academy of Sciences.* **112**, 54–59 (2015).
- 30 83. W. Zhong, D. J. Schwab, A. Murugan, Associative pattern recognition through macromolecular self-assembly. *J. Stat. Phys.* **167**, 806–826 (2017).
84. M. Imakaev, A. Goloborodko, H. B. Brandão, mirnylab/polychrom: v0.1.0 (2019), , doi:10.5281/ZENODO.3579473.

85. P. Eastman, J. Swails, J. D. Chodera, R. T. McGibbon, Y. Zhao, K. A. Beauchamp, L.-P. Wang, A. C. Simmonett, M. P. Harrigan, C. D. Stern, Others, OpenMM 7: Rapid development of high performance algorithms for molecular dynamics. *PLoS Comput. Biol.* **13**, e1005659 (2017).
- 5 86. J. C. Miller, T. Ting, EoN (Epidemics on Networks): a fast, flexible Python package for simulation, analytic approximation, and analysis of epidemics on networks. *Journal of Open Source Software.* **4**, 1731 (2019).
87. I. Z. Kiss, J. C. Miller, P. L. Simon, Others, Mathematics of epidemics on networks. *Cham: Springer.* **598**, 31 (2017).
- 10 88. J. Owen, *jaowen/3d-epigenetic-memory: First release* (Zenodo, 2023; <http://dx.doi.org/10.5281/ZENODO.8322781>).
89. P. Van Mieghem, Exact Markovian SIR and SIS epidemics on networks and an upper bound for the epidemic threshold. *arXiv preprint arXiv:1402.1731* (2014).
- 15 90. P. Van Mieghem, The N-intertwined SIS epidemic network model. *Computing.* **93**, 147–169 (2011).
91. B. Qu, H. Wang, The Accuracy of Mean-Field Approximation for Susceptible-Infected-Susceptible Epidemic Spreading. *arXiv preprint arXiv:1609.01105* (2016).
- 20 92. J. H. Gibcus, K. Samejima, A. Goloborodko, I. Samejima, N. Naumova, J. Nuebler, M. T. Kanemaki, L. Xie, J. R. Paulson, W. C. Earnshaw, L. A. Mirny, J. Dekker, A pathway for mitotic chromosome formation. *Science.* **359** (2018), doi:10.1126/science.aao6135.
93. R. Milo, R. Phillips, *Cell biology by the numbers* (CRC Press, Boca Raton, FL, 2015).
94. N. Naumova, M. Imakaev, G. Fudenberg, Y. Zhan, B. R. Lajoie, L. A. Mirny, J. Dekker, Organization of the mitotic chromosome. *Science.* **342**, 948–953 (2013).

Acknowledgments: The authors are very grateful to Mehran Kardar for valuable scientific discussions.

Funding:

National Human Genome Research Institute, NIH 3UM1HG011536 (LM)
National Institute of General Medical Sciences, NIH GM114190 (LM)
National Science Foundation 2044895 (LM)

Author contributions:

Conceptualization: JAO, DO, LM

Methodology: JAO, DO, LM

Investigation: JAO, DO, LM

Funding acquisition: LM

Project administration: LM

Supervision: LM

Writing – original draft: JAO, DO, LM

Writing – review & editing: JAO, DO, LM

Competing interests: Authors declare that they have no competing interests.

Data and materials availability: To simulate our model, we used polychrom (84), a lab-developed wrapper of OpenMM (85) for the polymer dynamics, and EoN (Epidemics on Networks) (86) for the mark dynamics. Code is available at <https://github.com/jaowen/3d-epigenetic-memory/> and deposited on Zenodo (88).

Supplementary Materials

Supplementary Text

Figs. S1 to S16

5 References (89 - 94)

Movie S1

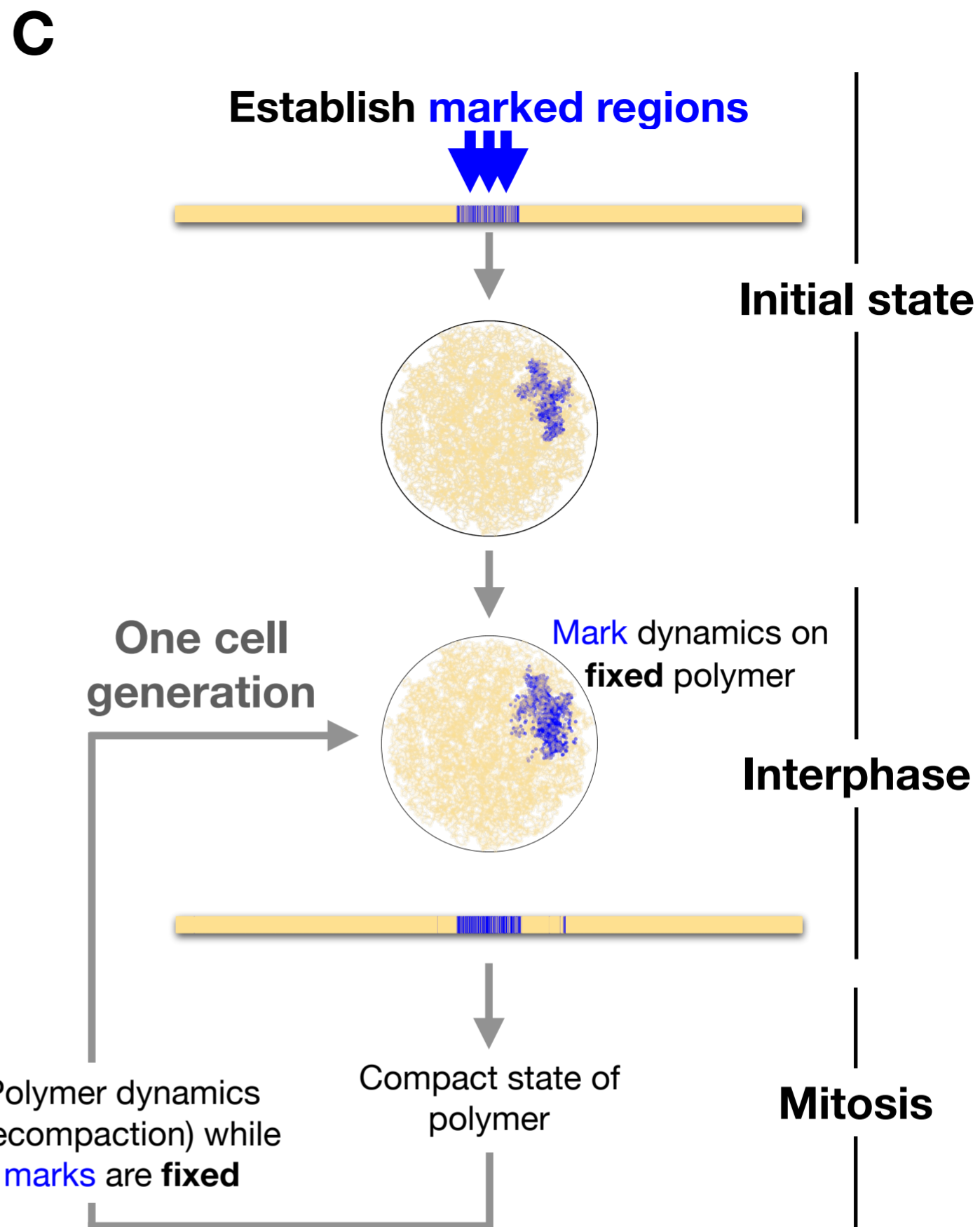
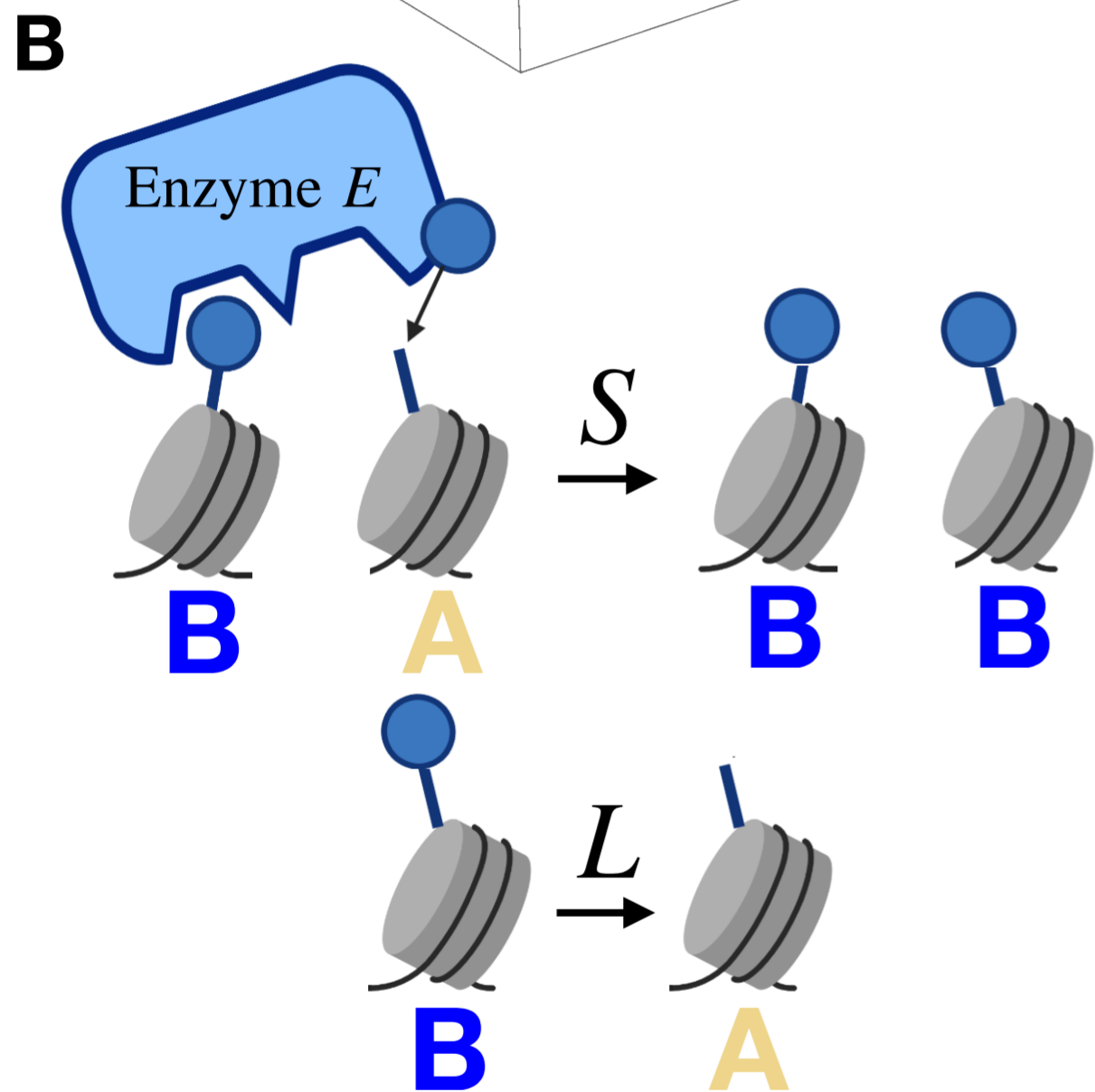
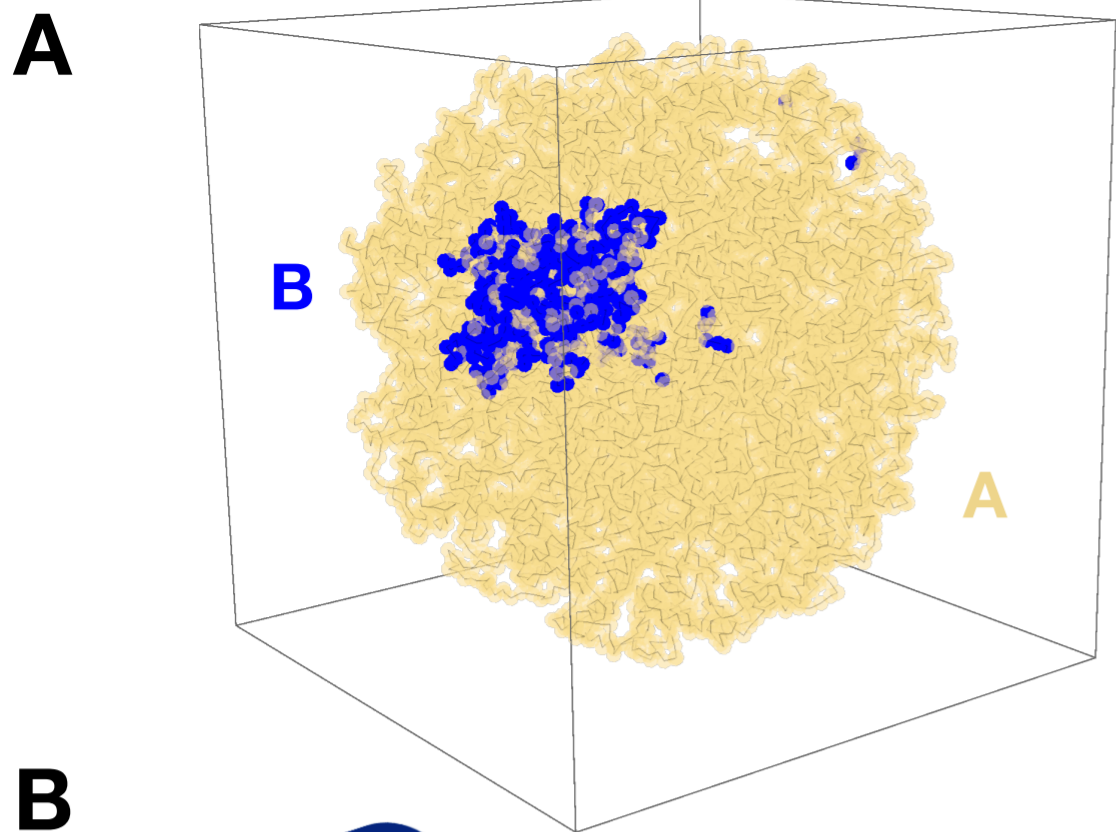
Fig. 1. Model of mark and chromatin dynamics. (A) Chromatin in the nucleus modeled as a spherically confined copolymer with monomers of two types, A (pale yellow) and B (blue), representing a varying pattern of histone marks. Monomers of type B, which represent regions bearing heterochromatic marks, self-attract. (B) Marks spread to 3D neighbors at rate S , and are lost everywhere uniformly at rate L . (C) The overall dynamics of our model consist of alternating phases of polymer dynamics and mark dynamics, representing the cell cycle.

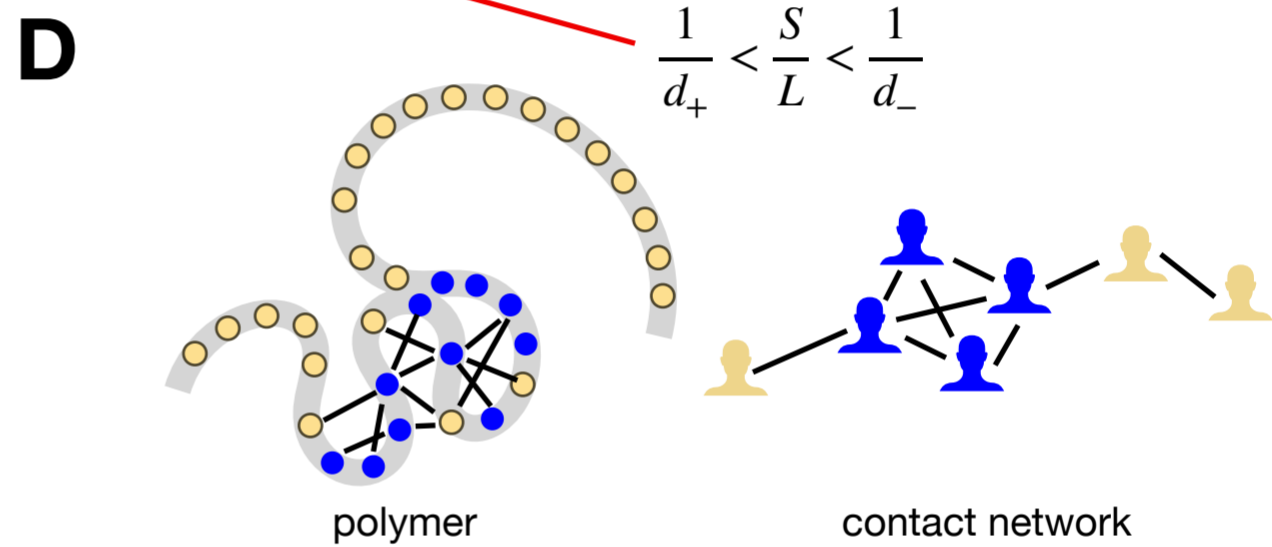
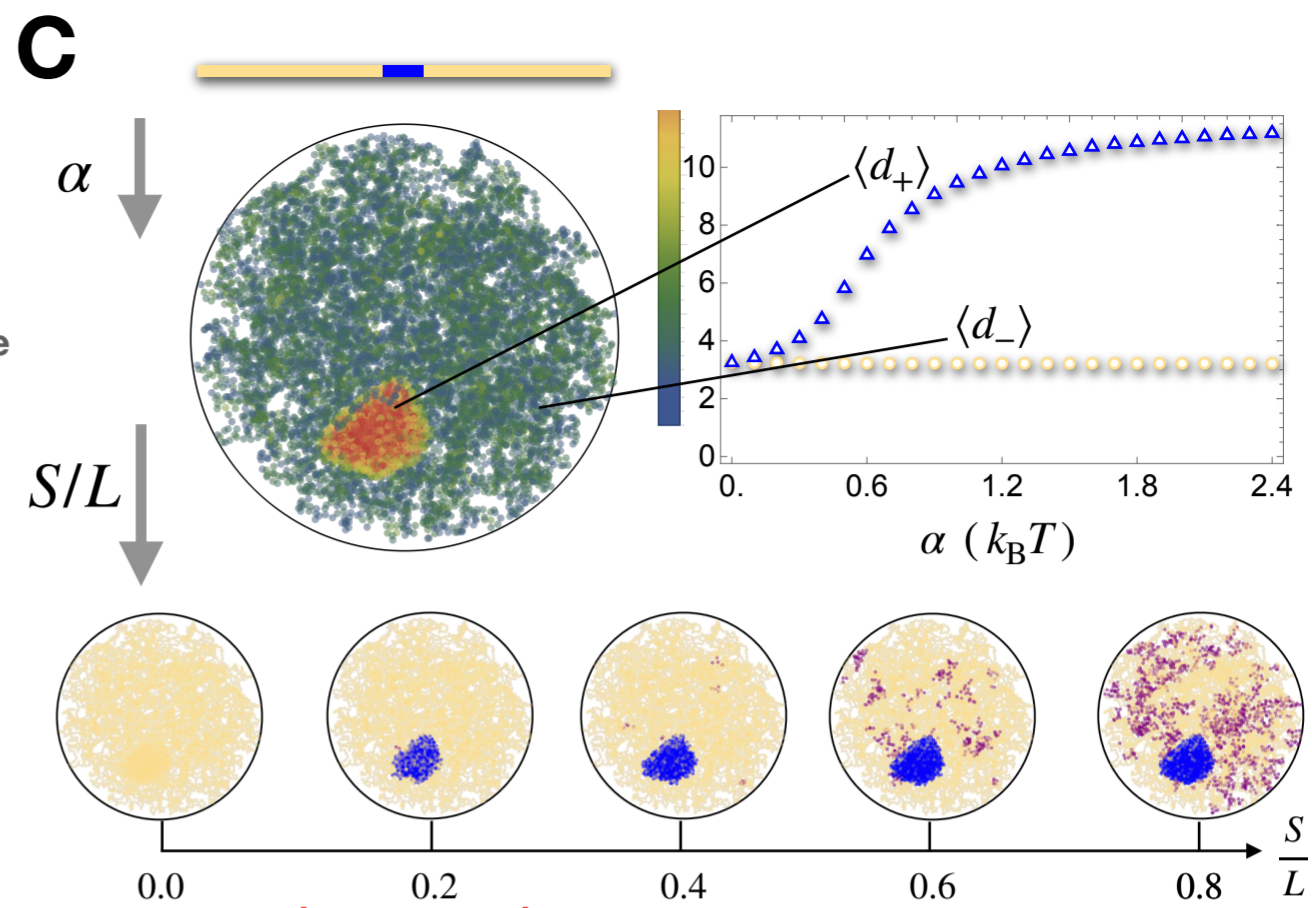
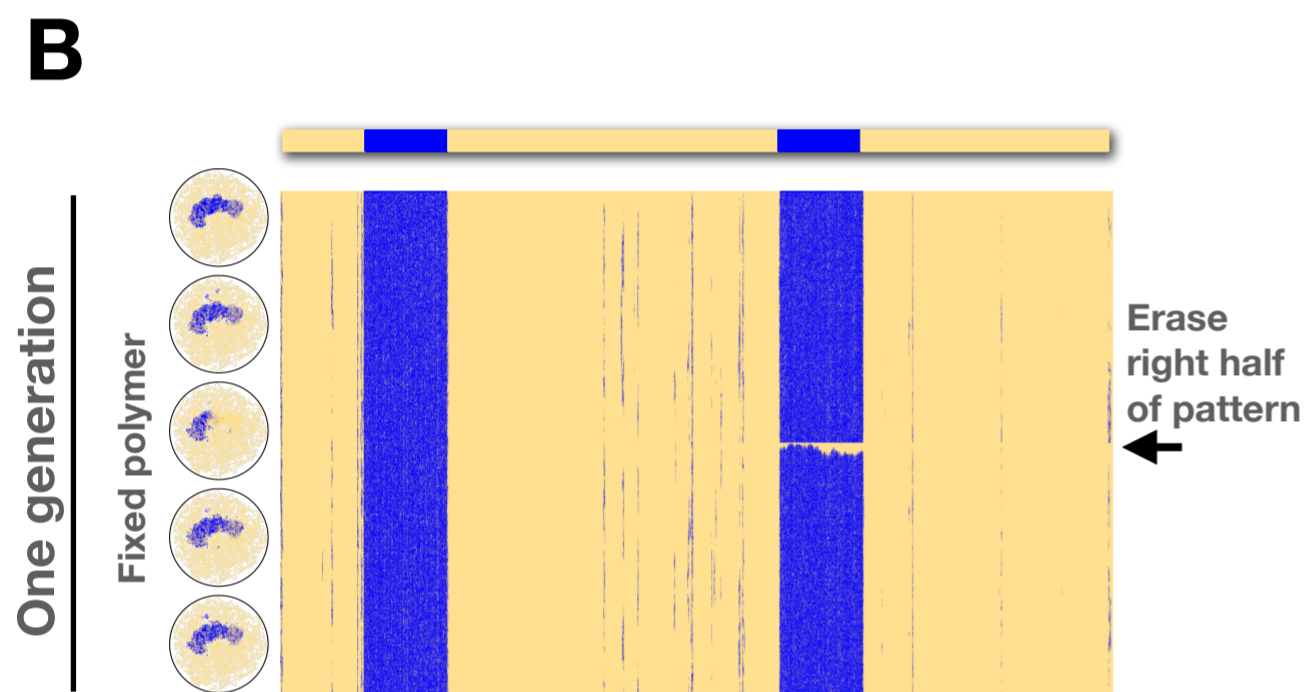
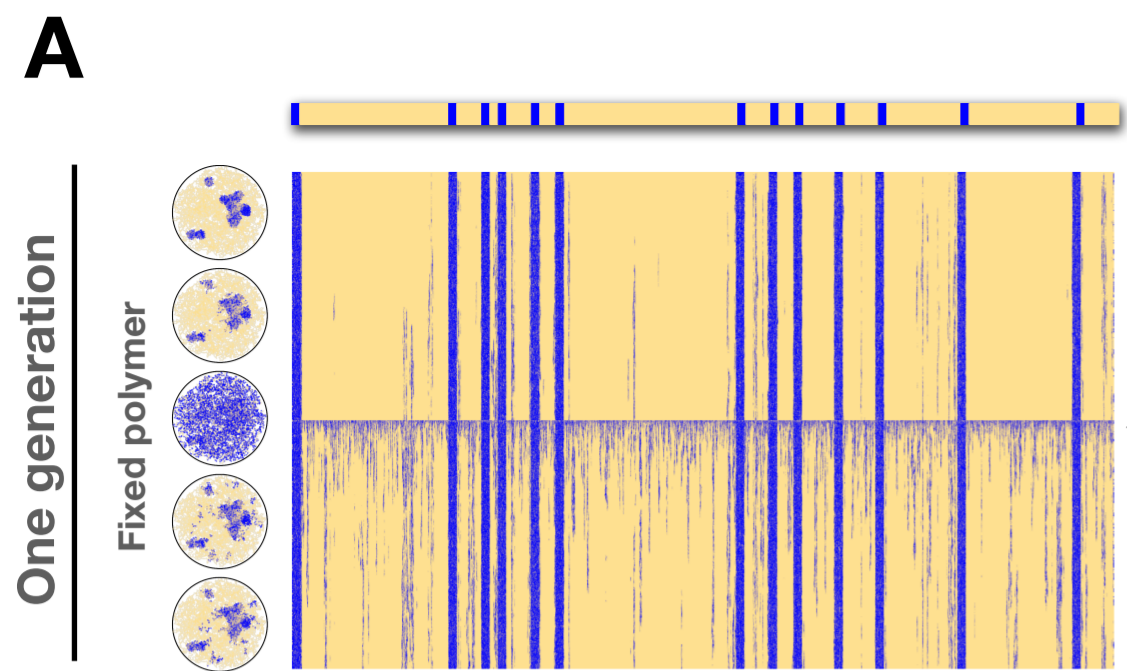
Fig. 2. Spreading marks sharply localize to dense regions. (A) Mark dynamics (with $S/L = 0.5$) over a single cell generation, on a fixed polymer folded according to an initial pattern (with $\alpha = 2.4 k_B T$). Time advances from top to bottom. Inset circles (left) show snapshots of the polymer configuration (2D projection) over time. (B) As in (A), with a different initial pattern and perturbation. (C) Top: when the polymer folds, marked regions tend to be denser (red) than unmarked ones (green), due to the self-attraction of marks. The plot shows the average number of monomer neighbors in each compartment as a function of the strength of B-B self-attraction α . Bottom: in turn, when marks evolve according to their dynamics of spreading and loss, they tend to localize in dense regions for a range of S/L values. (D) An analogy to epidemic spreading, where marked monomers are equivalent to infected people, predicts correctly that this localization will occur *at least* in the red interval, whose width is set by the number of neighbors in each region.

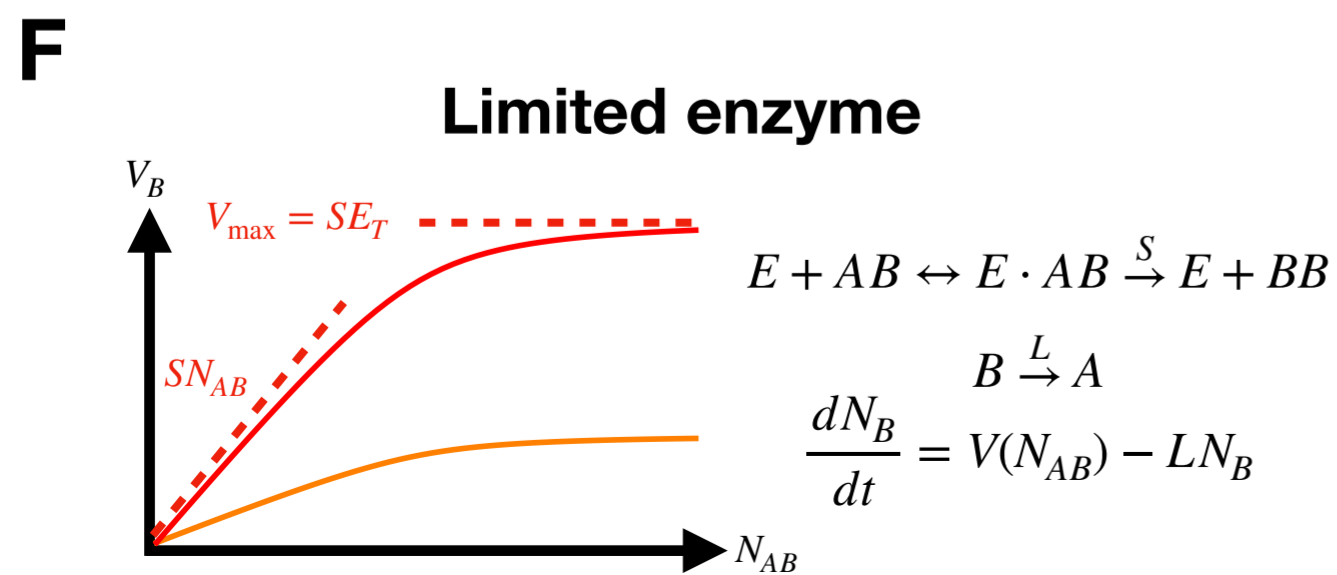
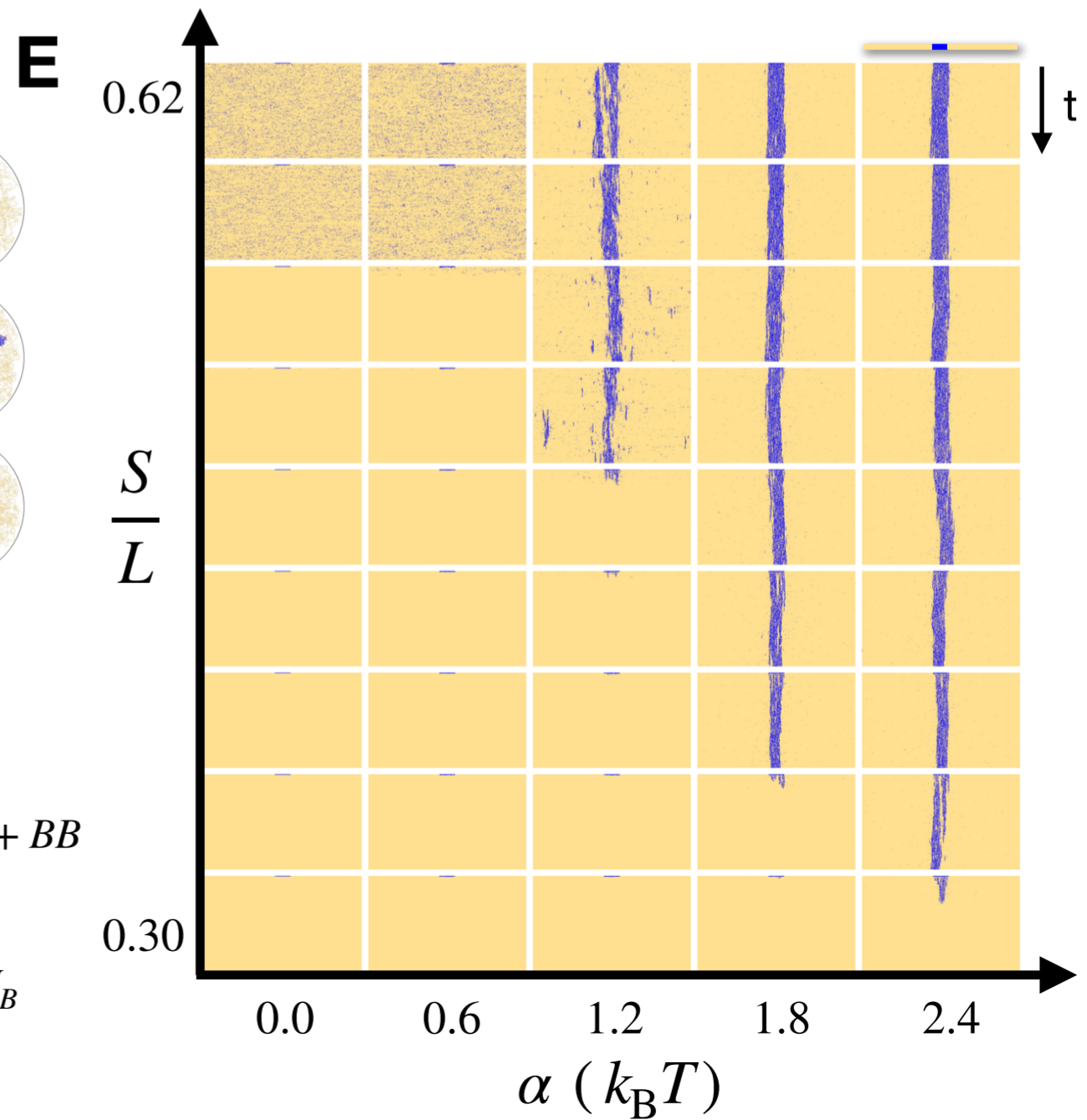
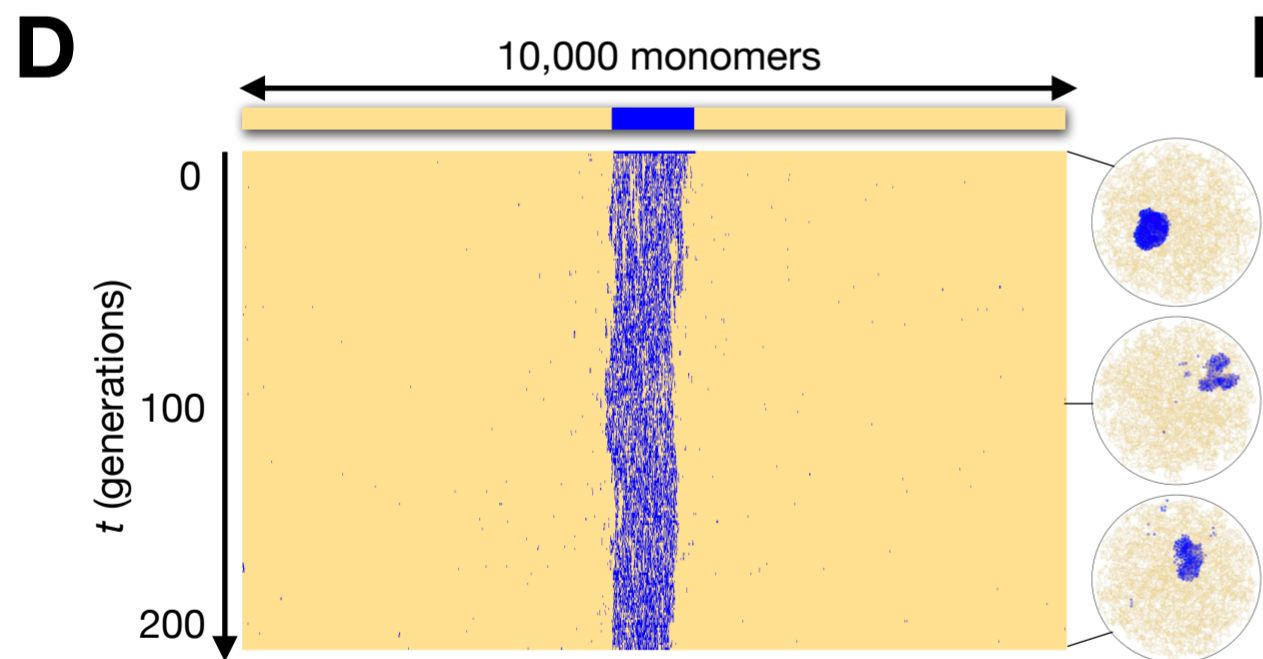
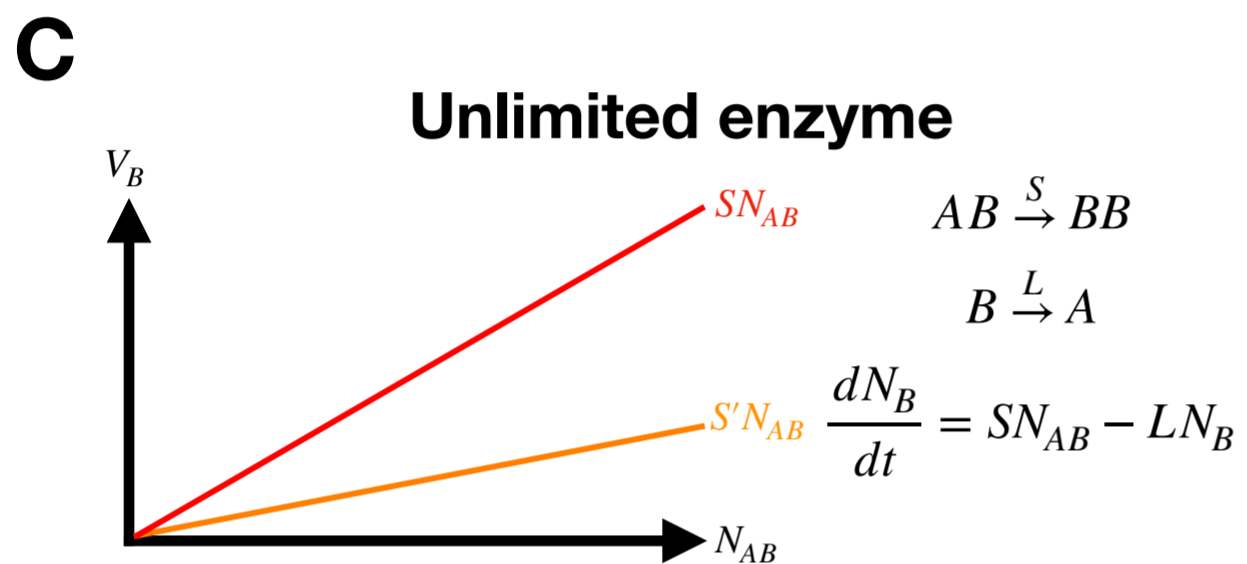
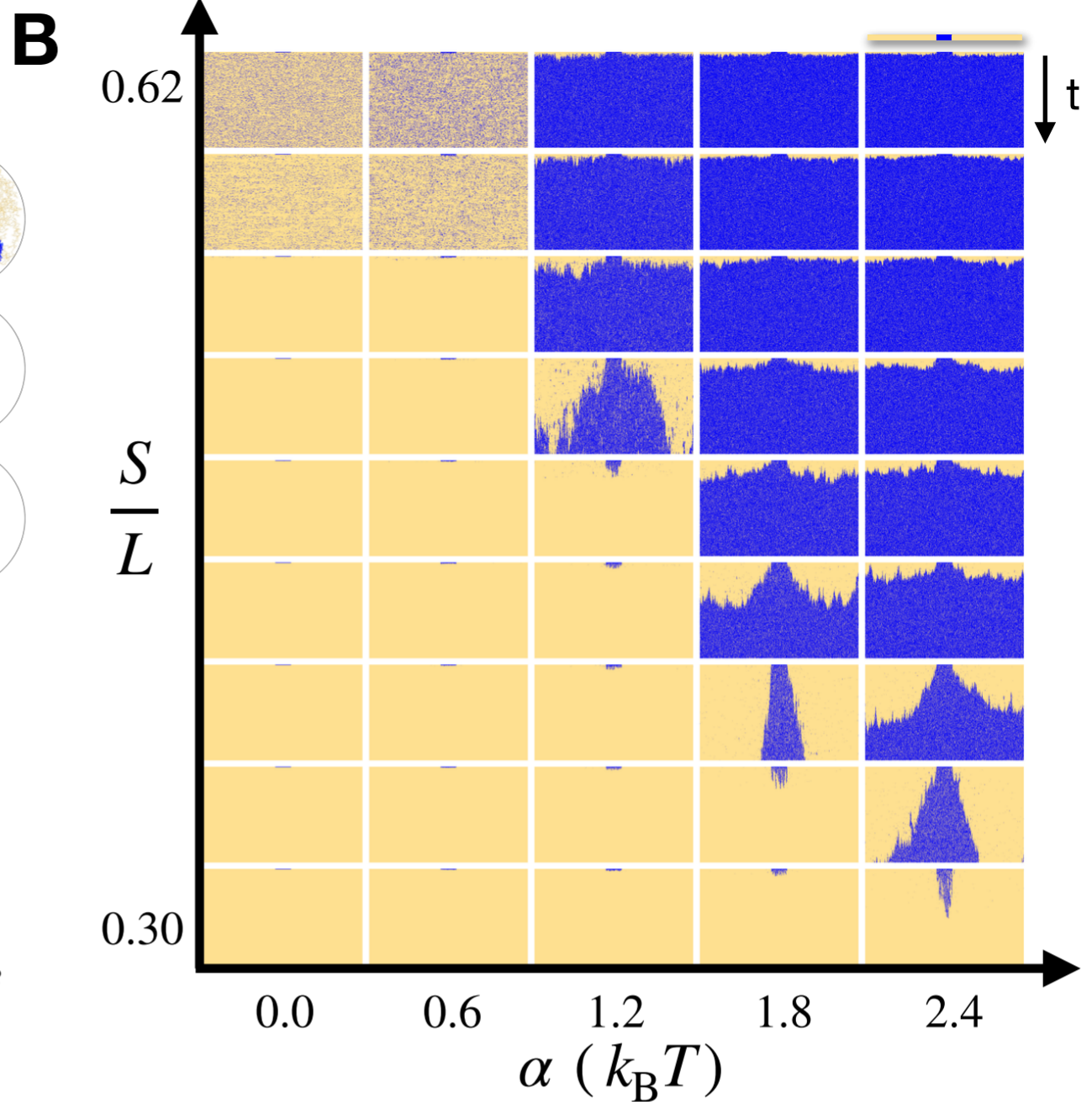
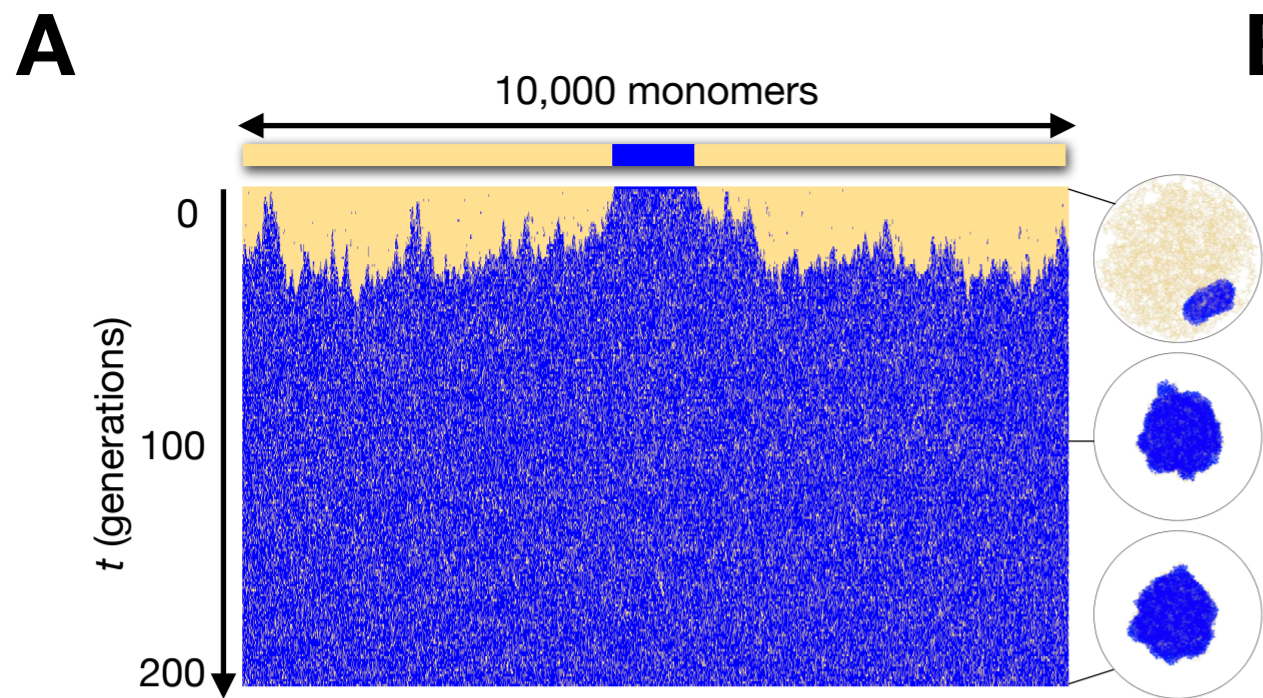
Fig. 3. Limited enzyme stabilizes memory over multiple generations. (A) Time evolution of a mark pattern, with unlimited enzyme, over 200 generations ($\alpha = 2.4 k_B T$, $S/L = 0.42$), starting from an initial pattern consisting of a single domain of 1000 marked monomers. Inset circles show snapshots in time of the polymer configuration. For this choice of parameter marks spread everywhere and the polymer collapses. (B) Time evolution of the mark pattern, with unlimited enzyme, as a function of α and S/L . No stable memory. (C) With unlimited enzyme, the global marking rate in the nucleus V_B is proportional to the number N_{AB} of A-B pairs. (D) and (E), just as in (A) and (B), but with limited enzyme, $E_T = 1000$. Stable memory is achieved for hundreds of generations, over a broad range of parameters. (F) With limited enzyme, V_B is proportional to N_{AB} when it is small, but then saturates at the value $V_{\max} = SE_T$, preventing uncontrolled spreading of marks.

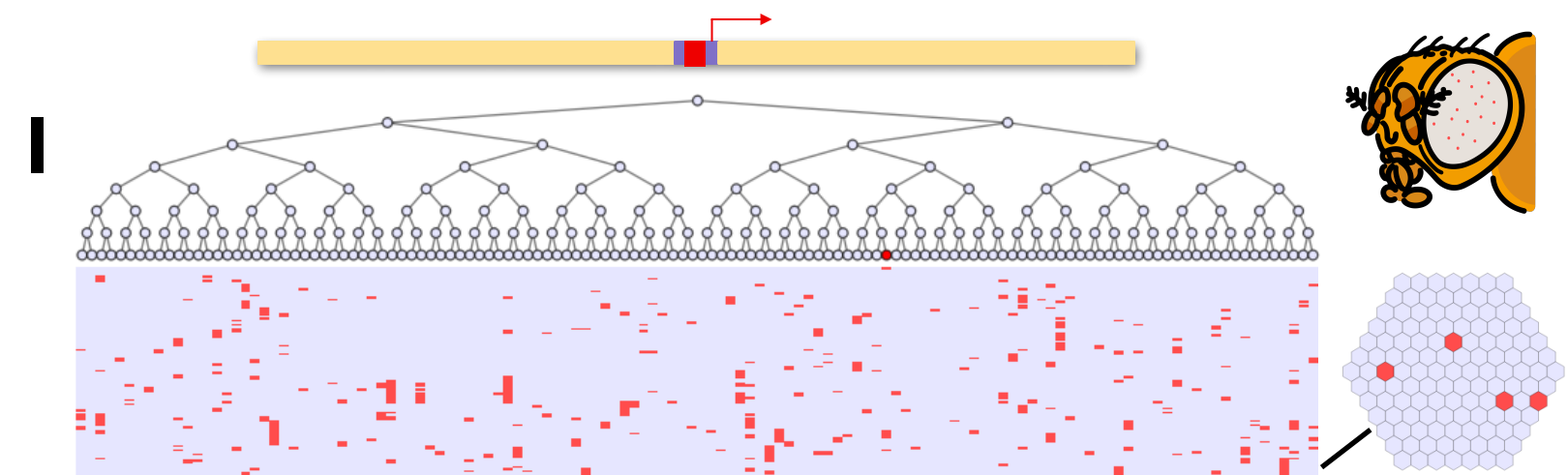
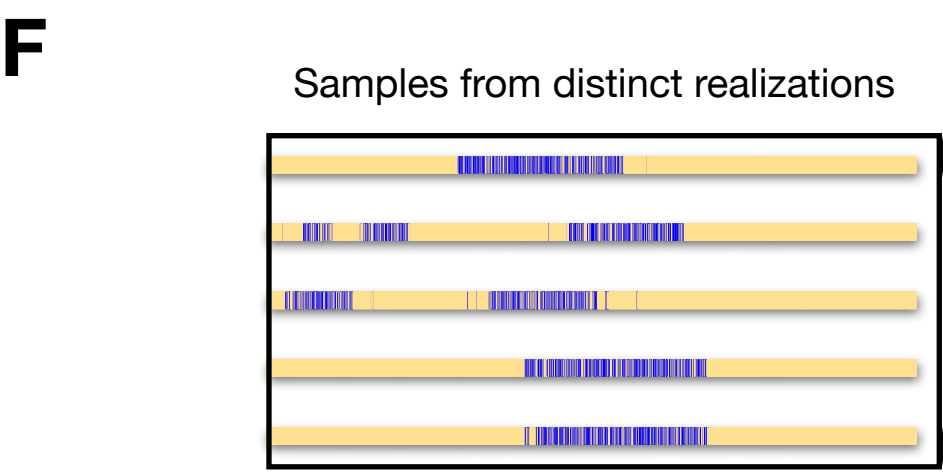
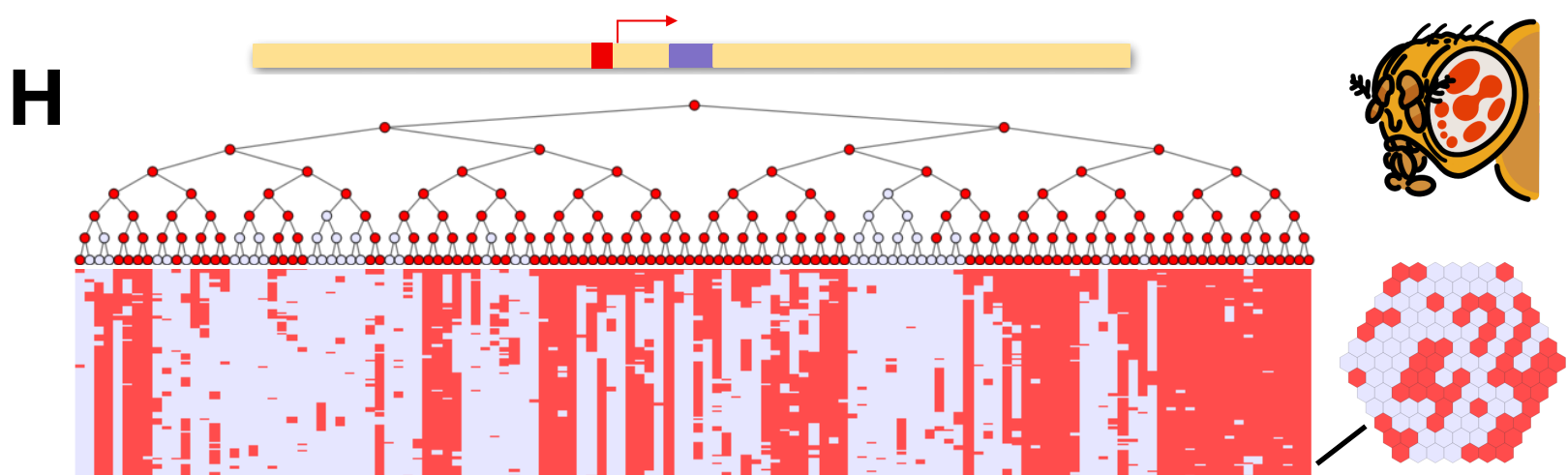
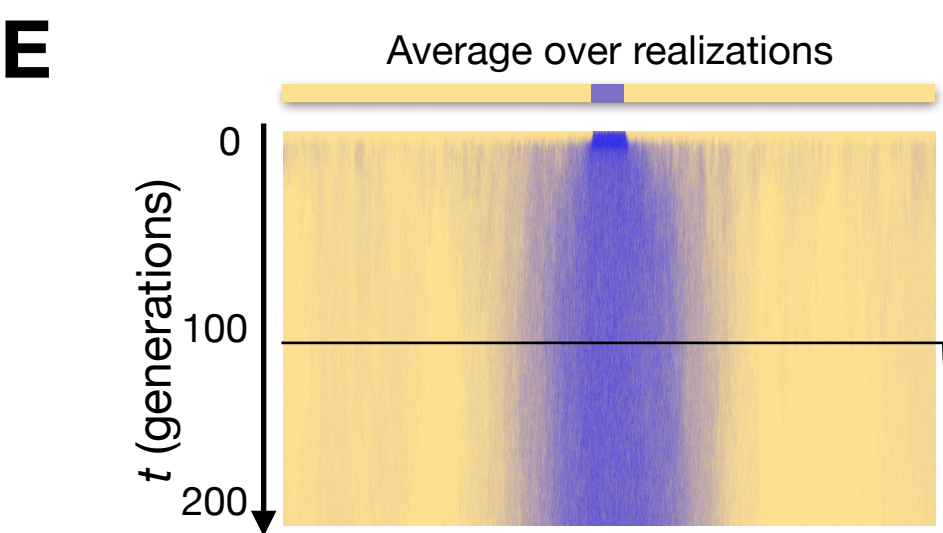
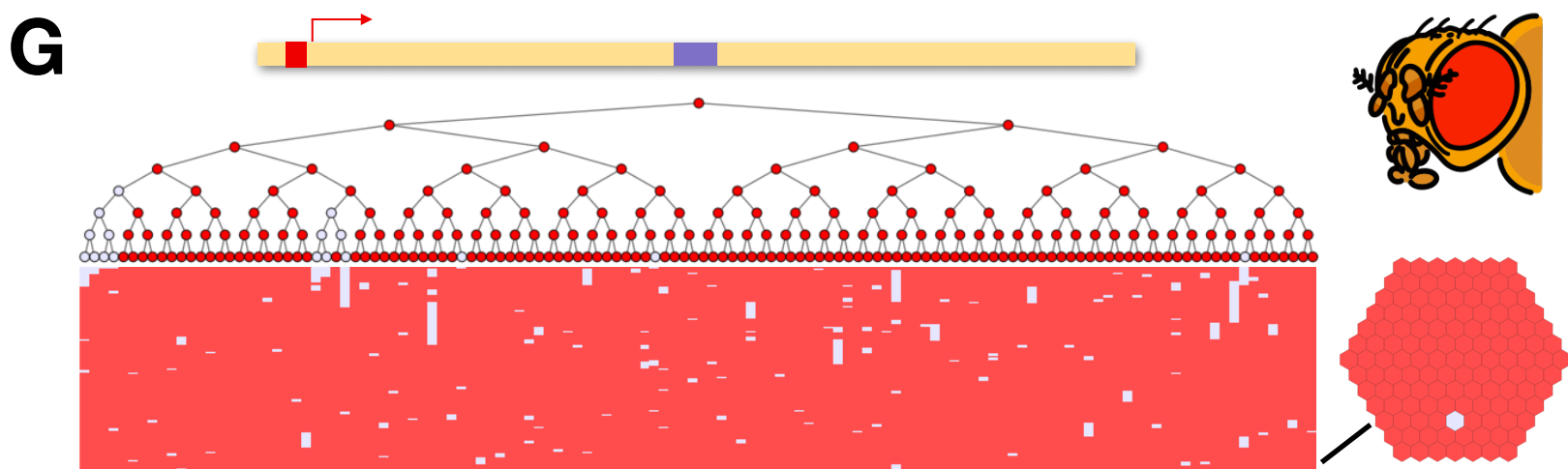
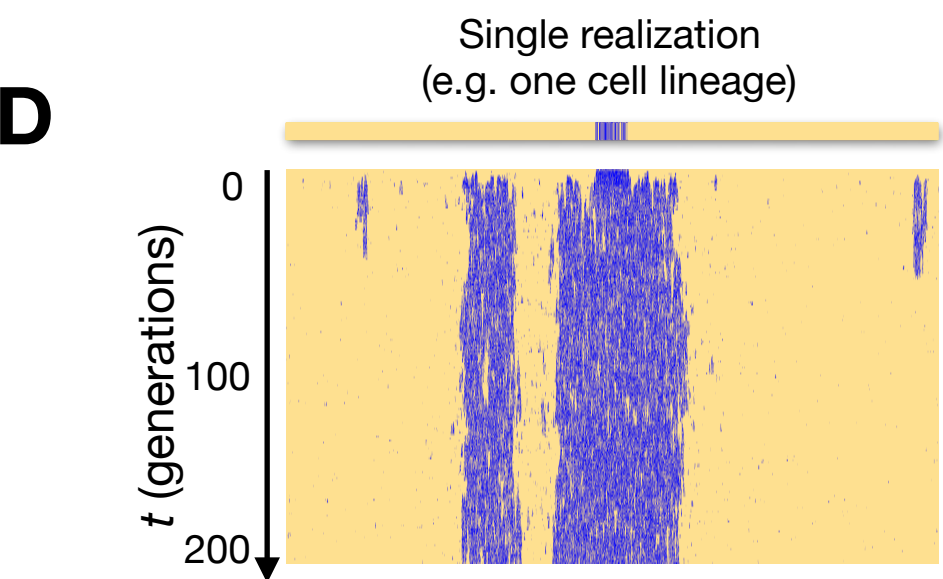
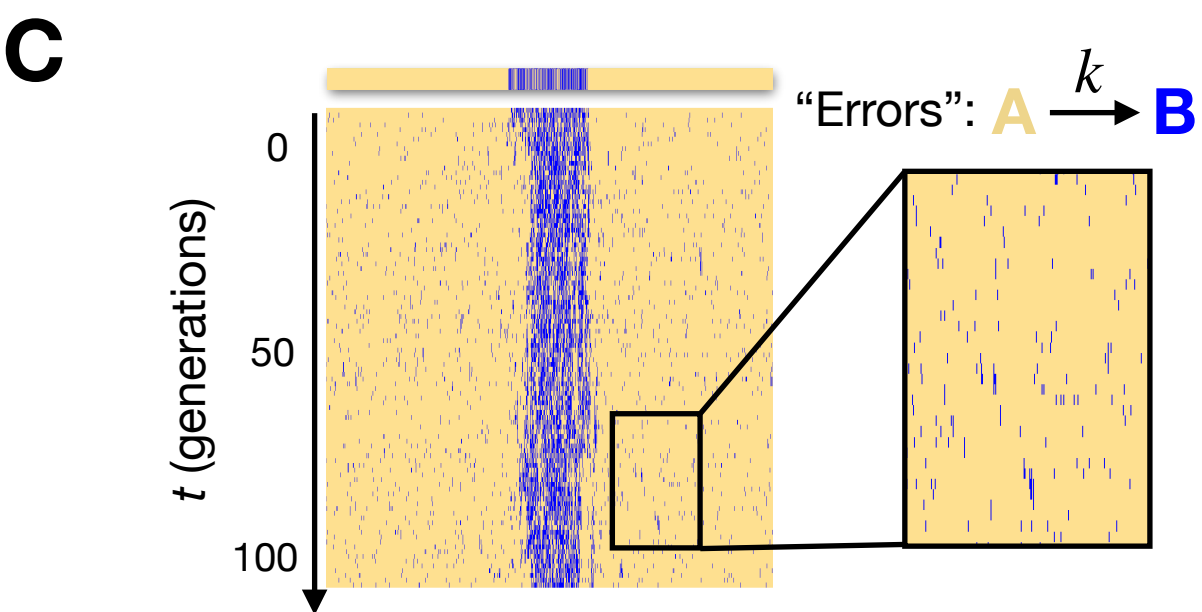
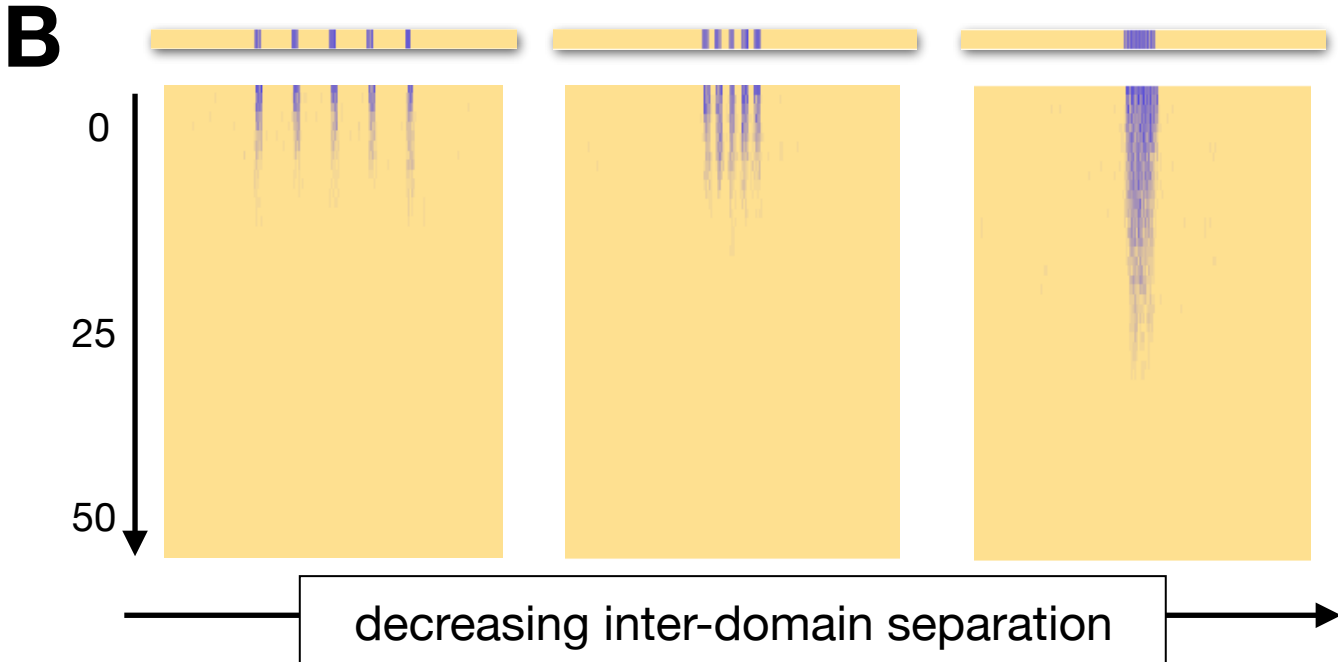
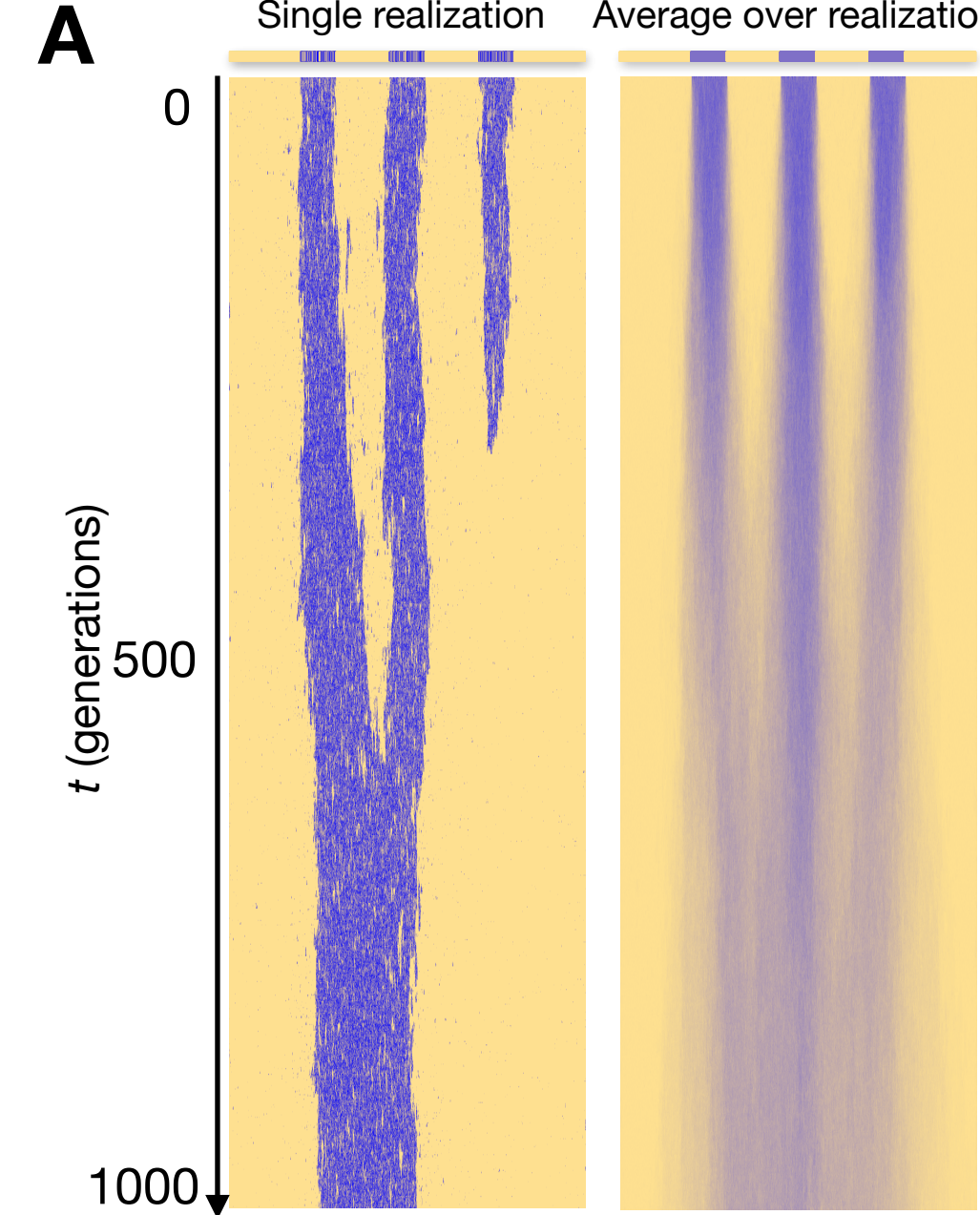
Fig. 4. Dynamics of complex patterns and position-effect variegation. (A) Time evolution of a pattern consisting of three, equally-sized mark domains ($\alpha = 2.4 k_B T$, $S/L = 0.5$, $E_T = 3000$). The pattern is stable for hundreds of generations, though marks eventually redistribute to form a single contiguous domain. In a population average (right) the three domains instead appear to merge. (B) Multiple small domains ($\alpha = 2.4 k_B T$, $S/L = 0.5$; population average shown) competing with a much bigger one (not pictured) survive redistribution longer the closer they are together. (C) Error correction: tiny “domains” introduced by spontaneous marking at a rate k are lost immediately ($\alpha = 2.4 k_B T$, $S/L = 0.5$, $E_T = 1000$, $k/L = 0.003$). (D) Expansion of marks

from a small domain leads to the random formation of new domains that can be remembered for hundreds of generations ($\alpha = 2.4 k_B T$, $S/L = 0.5$, $E_T = 3000$). **(E)** The population average of **(D)** hides the large cell variation **(F)**. **(G-I)** Position-effect variegation: To visualize the consequences of this, we consider a gene “regulatory region” of five consecutive monomers (red), somewhere along the polymer, and take the presence of a single B monomer in this region to silence the gene. Investigating silencing status (white = silenced, red = not silenced) in a lineage tree generated with our model, we find different phenotypes reminiscent of the classic position-effect variegation: **(G)** wild-type, **(H)** “sectored” variegation, and **(I)** “salt-and-pepper” variegation, depending on the position of the regulatory region.











5
Supplementary Materials for
Design principles of 3D epigenetic memory systems

Jeremy A. Owen, Dino Osmanović, Leonid Mirny

10
Correspondence to: leonid@mit.edu

15
This PDF file includes:

Supplementary Text
Figs. S1 to S16

20
Other Supplementary Materials for this manuscript include the following:

Movie S1

25

30

Supplementary Text

Mean-field theory for mark dynamics on a spatial network with a dense region

Consider our mark dynamics—or completely equivalently, an SIS (Susceptible-Infected-Susceptible) epidemic model—on a (undirected) graph G with adjacency matrix A . For us this is a model of a covalent chemical modification (a “mark”) spreading between monomers of a frozen polymer. Marks spread between adjacent monomers at rate S and are lost everywhere at rate L .

Let X_i be a random variable which takes the value 1 if the i th monomer is marked and takes the value 0 if the i th monomer is not marked. The expectation value of X_i obeys the differential equation (89):

$$\frac{dE(X_i)}{dt} = E \left[S(1 - X_i) \sum_j A_{ij} X_j - LX_i \right].$$

Note that this cannot be turned into a closed equation for $E(X_i)$ since the X_i are not independent variables in general, $E(X_i X_j)$ is not equal to $E(X_i)E(X_j)$. However, it turns out that it is true (for this model) that $E(X_i X_j) \geq E(X_i)E(X_j)$ —a mark on one monomer can only ever make it *more* likely that another monomer is marked. Therefore,

$$\frac{dE(X_i)}{dt} \leq S \sum_j A_{ij} [E(X_j) - E(X_i)E(X_j)] - LE(X_i).$$

The assumption of equality in the equation above is a mean-field approximation called the N -intertwined mean-field approximation (NIMFA) (90). Importantly, the accuracy of NIMFA appears to increase (e.g., the inequality above becomes closer to equality) as the steady-state mark probabilities $E(X_i)$ increase (91).

Now suppose G is a regular graph—one where every single node has the same number of neighbors (or degree) d . Let’s also focus on the *steady-state* of the SIS model, reached after a

long time, and suppose that in that steady-state, the probability of any site being marked is the same as that of any other—i.e., $E(X_i) = p$ for all i . Then, we have

$$0 \leq Sdp(1 - p) - Lp$$

which means that either $p = 0$ or:

$$p \leq 1 - \frac{L}{Sd}$$

And so according to NIMFA, p is approximately $\max(1 - L/(Sd), 0)$, and this approximation gets better as p increases.

Now suppose we have a network with a dense region where a typical node has d_+ neighbors and a diffuse region where a typical node has d_- neighbors.

A very crude approach to understanding the behavior of the steady-state mark probability on this network is to treat these two regions as independent, regular graphs with degrees d_+ and d_- , respectively. Given this (admittedly very strong), simplifying assumption, we would expect that the steady-state mark probability in the dense region satisfies $p_+ \leq \max(1 - \frac{L}{Sd_+}, 0)$ and that in diffuse region we have $p_- \leq \max(1 - \frac{L}{Sd_-}, 0)$.

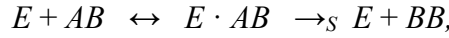
But, if the dense region is dense *enough*, then NIMFA is a good approximation there, and we have $p_+ \approx 1 - \frac{L}{Sd_+}$ while in the diffuse region we still have $p_- \leq \max(1 - \frac{L}{Sd_-}, 0)$. And so, in this regime, there is a range of values of S/L :

$$\frac{1}{d_+} \leq \frac{S}{L} \leq \frac{1}{d_-}$$

in which there are marks in the dense region but very few (in the approximation, none) in the diffuse region.

Modeling limited enzyme

Consider a Michaelis-Menten-like enzyme E that binds to AB pairs and then (once bound) converts them to BB pairs, e.g.,



where $E \cdot AB$ is an intermediate complex, and S is the rate constant for the catalysis step. The instantaneous rate V_B of catalysis (the creation rate of B), globally (e.g., in the whole nucleus) is

$$V_B = S [E \cdot AB].$$

Suppose the formation of the complex is very fast and can be assumed to always be at equilibrium, so that

$$\frac{[E][AB]}{[E \cdot AB]} = K_D,$$

where K_D is a dissociation constant. The total enzyme concentration $E_T = [E] + [E \cdot AB]$ is always conserved. On the very fast timescale of complex formation, the total number $N_{AB} = [AB] + [E \cdot AB]$ of AB pairs is also approximately conserved, which leads to

$$\frac{[E \cdot AB]}{N_{AB}} \approx \frac{E_T + K_D + N_{AB} - \sqrt{(E_T + K_D + N_{AB})^2 - 4N_{AB}E_T}}{2N_{AB}}.$$

Finally, let's suppose the binding of the enzyme to AB pairs is very strong, so that $K_D \rightarrow 0$.

In this limit, we find

$$\frac{[E \cdot AB]}{N_{AB}} \rightarrow 1$$

when $N_{AB} \leq E_T$, and

$$\frac{[E \cdot AB]}{N_{AB}} \rightarrow \frac{E_T}{N_{AB}}$$

when $N_{AB} > E_T$.

Subject to these assumptions of timescale separation and strong enzyme binding, we therefore find that *for any given AB pair*, there is an effective spreading rate S_{eff} :

$$S_{\text{eff}} = \frac{V_B}{N_{AB}} = \frac{S [E \cdot AB]}{N_{AB}} = \begin{cases} S & \text{if } N_{AB} < E_T \\ \frac{SE_T}{N_{AB}} & \text{if } N_{AB} \geq E_T \end{cases}.$$

Modeling the loss of marks

In all the main text results, we model loss of marks as conversion of B monomers into
5 A monomers at a constant rate L , uniformly at all sites. However, all marks are diluted by
newly synthesized, unmarked histones when DNA is replicated in S phase. For some marks,
this could be the main loss mechanism. To confirm that our results do not depend on the
precise way loss is modeled, we investigated a variant of our model where marks only spread
during interphase (no constant loss), except for the loss of a random 50% of the marks halfway
10 through the interphase (modeling replicative dilution). Since marks can no longer relax during
interphase (their number only ever growing, due to spread), the interphase duration T_{div} (the
time between cell divisions) becomes a key model parameter.

The dilution-only model can be compared to the constant loss model by matching the
half-life of the marks in the two models, defining an effective loss rate for the dilution-only
15 model of $L_{\text{eff}} = T_{div}/\log(2)$ so that $\exp(-L_{\text{eff}}T_{div}) = 1/2$. In Figure S2, we show the
behavior of the dilution-only model as S/L_{eff} and α are varied, finding it to be very close to
that of the constant loss model (Figure S2).

Modeling mitotic spread

20 For the variant of our model which includes mitotic spread of marks, we start with the
version of our model (described above), where marks are lost solely by replicative dilution.
We first create (every model generation) a contact graph G_M to represent the mitotic
chromosome. The vertices of G_M are all the monomers and there is an edge between any two

monomers with probability f_{dens}/\sqrt{s} , where s is the distance between the monomers along the polymer, roughly matching the contact probability scaling for the mitotic chromosome observed in Hi-C experiments (92). f_{dens} is a scaling factor to control the average number of neighbors in the mitotic state—chosen so as to achieve a 3-fold densification of the mitotic chromosome relative to B regions when $\alpha = 2.4$. Given that the global volume fraction of monomers in our model is 5%, and our B regions are 3 times denser than that, this corresponds to a “mitotic chromosome” with a monomer volume fraction of 45% (compare to the estimate of 40% used in (92)).

Between every “interphase”, before the polymer refolds, we allow marks to spread on the “mitotic” contact graph G_M for a time T_{mito} , with spreading rate Sf_{ac} . As our key control parameters, we vary f_{ac} and the duration of mitosis relative to that of the whole cell cycle $T_{\text{mito}}/T_{\text{div}}$.

We find that mark domains can remain stable even if mitotic spread is possible (Figure S3B). Notably, for realistic durations of mitosis (e.g., 5% of the whole cell cycle), domains remain stable even if the accessibility factor $f_{\text{ac}} = 1$, i.e., if spread of marks is *just as easy* on the mitotic chromosome as it is in interphase. This stability is a consequence of limited enzyme, because even though the mitotic chromosome is much denser, and there are many more contacts, enzyme limitation means that marks are always made at the same rate. If enzyme were unlimited (Figure S3D), the increased density in the mitotic state would stimulate marking at a much higher rate, leading to catastrophic spread of marks despite the short duration of mitosis. This further reinforces the importance of limited enzyme as a key ingredient for epigenetic memory.

If the accessibility of mitotic chromatin, or the activity of reader-writer enzymes, is reduced ($f_{\text{ac}} < 1$), the effects of mitotic spread become even smaller (Figure S3B).

Modeling interphase chromatin dynamics

To model interphase chromatin dynamics, we divide the mark dynamics in each interphase into 200 short segments, which are interlaced with 200 short movements of the polymer (each consisting of some number T of timesteps of the Brownian integrator of OpenMM). The resulting time evolution of the mean-squared displacement (MSD) of a monomer has an early diffusive regime ($\text{MSD} \sim t$) that later crosses over to a Rouse-like regime ($\text{MSD} \sim t^{1/2}$). The latter has been as observed by Gabriele et al. in recent locus-tracking experiments (32), where they measured dynamics for times on the order of 1000 seconds, and fit their MSD data to $\Gamma t^{1/2}$, finding $\Gamma = 0.0024 \mu\text{m}^2/\text{s}^{1/2}$.

To roughly match the scale of our simulated dynamics to reality, we assume an interphase duration of 24 hours and that the sphere confining our polymer represents a cell nucleus with a diameter of 10 micrometers. We choose the number of timesteps T in each segment to match the prefactor Γ of our Rouse-like regime to experimentally measured values. This matching procedure results in an unrealistically late crossover between the diffusive to Rouse regimes, compared to reality. This is a consequence of the coarse-grained nature of our polymer model. The crossover can be expected to occur after diffusion over a distance related to the bond length, but in our model (since there are relatively few monomer) this is an appreciable fraction of the nuclear diameter.

We believe that matching our model's dynamics to the locus-tracking experiments may result in an exaggerated degree of simulated chromatin motion over the whole interphase. This is because we are effectively extrapolating dynamics observed over 1000 seconds to much longer times, when we expect dynamics to slow down due to effects such as chromosome territoriality.

This variant of our model (Figure S4B) exhibits stable mark domains, although interphase dynamics accelerates their slow diffusion along the polymer (over 100s of generations).

This illustrates that “freezing” of chromatin during interphase is not required—our mechanism is compatible with a realistic degree of interphase dynamics. However, in these simulations, mark dynamics are still very fast relative to polymer motion. To probe a regime where mark dynamics are slower relative to polymer motion, we apply interphase dynamics to our dilution-only model. Since all marks must *at least* be lost by replicative dilution, this model represents, in some sense, the slowest mark dynamics possible. When $\alpha = 2.4$ kT in this model, we find that contiguous mark domains are not stable. This behavior is strongly reminiscent of the dilution-only model without interphase dynamics when α is too low to sustain stable memory. Inspired by this, we increased α to 4.8 kT, which indeed rescues the memory of marked domains (Figure S4C).

Modeling nucleation regions and transcriptional antagonism

We model nucleation regions (Figure S11) as stretches of permanent B monomers (monomers for which we set $L = 0$). To minimally capture transcriptional antagonism, we introduced unmarkable regions (Figure S12) to our polymer—stretches of permanent A monomers (spread of marks to them is impossible). We still allow the enzyme to bind (unproductively) to the AB pairs formed when a B monomer is within the interaction radius of an unmarkable A monomer.

A lower bound on the memory capacity of our model

Our model exhibits memory in the sense that evolving mark patterns can resemble the initial pattern for many generations, for many different choices of the initial pattern. But to quantitatively estimate the memory capacity, we need to define when two patterns are to be considered the “same”, because the initial pattern is never preserved *precisely*, even for a single generation (for example, our model is not suited to remember the marking status of one particular monomer). To this end, we divide up our polymer (of length N) into N/w contiguous “bit-regions” of length w (Figure S13A). We can convert any mark pattern into a length N/w bit-string by reading out a bit-region as a “1” if more than 25% of the monomers in the region are marked, and as a “0” otherwise. We identify two patterns with each other if they map to the same bit-string. We can then ask how long a random bit-string can be remembered by our model.

To initialize our system, we choose a random bit-string and set the bit-regions corresponding to 1s to be 50% marked, and the bit-regions corresponding to 0s to be totally unmarked. Since we do not want to specialize the enzyme concentration E_T to each bit-string, we exclusively use bit-strings with equal numbers of 1s and 0s. This means the initial number of marks is functionally the same for all initial patterns.

We then evolve the initial pattern for 50 generations using our model ($\alpha = 2.4$, $S/L = 0.5$, $E_T = 5000$), map the patterns to bit-strings, and observe the appearance of errors as marks tend to redistribute to form contiguous domains. For fixed w , we compute the growth of the error probability averaged over many random initial bit-strings (Figure S13B).

What we find is a tradeoff between w (the width of the bit-regions) and the rate at which errors appear. The wider the bit-regions, the more stable the memory. This effect is clearly related to our observation that longer domains are more resistant to mark redistribution (Figure S9A). This implies a tradeoff between the *capacity* of our memory system and the

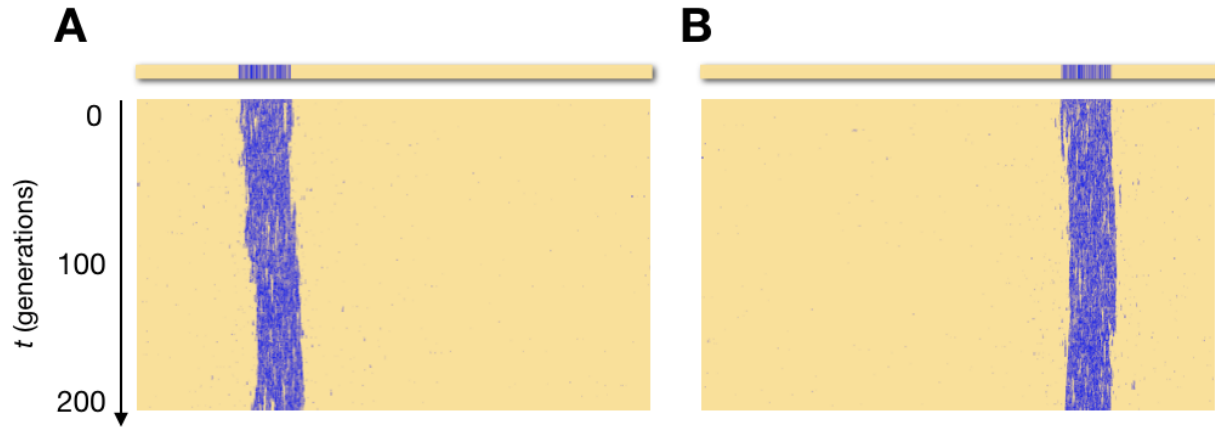
stability of the memory. Naively, the capacity (in bits) of this scheme would just be the number of bit-regions N/w . However, since we only start with bit-strings with equal numbers of 0s and 1s, our capacity is a little less—it is log base 2 of the number of those possible initial states, which is $\text{Binomial}(N/w, N/2w)$. Just like N/w , this decreases in w , which means that the higher the capacity we desire (lower w), the faster errors will appear (less stability). To quantify stability, we can ask after how many generations the error probability exceeds a threshold. We find a reciprocal relationship between this time and the capacity (Figure S13C).

Tests of predicted relationship between E_T , S/L and the number of marks

Our limited enzyme model predicts that when a mark made by a reader-writer enzyme persists (e.g., when S/L is above the critical value), the number of marks N_B should be linearly related to S/L and enzyme concentration E_T according to $N_B = SE_T/L$. Our impression is that data to convincingly test this have not yet been reported in the literature. To test the relationship, the abundance (or activity) of a reader-writer enzyme, as well as the abundance of an epigenetic mark, must be carefully measured while the former is varied over a range of values. Additionally, many complicating factors, such as nucleation regions for marks, marks acted on by multiple enzymes, or feedback from downstream effects of changes in marks, could cause violations of this linear relationship.

Nevertheless, existing data is consistent with our predicted relationship. For example, McCabe et al. (44) reported on the effects of GSK126—a SAM-competitive EZH2 inhibitor—on H3K27me3 levels in cells. For several different cell lines, they report the concentration IC50 of GSK126 required to reduce by half the H3K27me3 abundance (quantified by ELISA). They also report the IC50 of the GSK126 acting on PRC2, measured using *in vitro* methyltransferase assays. If EZH2 is presumed completely inactive when bound by GSK126,

then titrating the inhibitor is just like changing the enzyme concentration, and our model would predict that these two IC50s (for H3K27me3 reduction *in vivo*, and for PRC2 inhibition *in vitro*) should be the same. Assuming an intracellular SAM concentration of ~ 0.2 mM (93), extrapolating their *in vitro* measurements (Supplementary Figure 1 in (44)) implies a IC50 of
5 around 300 nM, which is indeed close to what they found in two of their cell lines (Figure 1c in (44)). In this picture, variation between cell lines in their sensitivity to GSK126 could be explained by variations in the intracellular SAM concentration.



5

10

Fig. S1. Positional memory. The memory in our model, in the limited enzyme regime, is one of domain position. This is illustrated in panels (A) and (B), which show two realizations of our model with identical parameters ($\alpha = 2.4$, $S/L = 0.50$, $E_T = 1000$), but different initial positions of a single contiguous domain of marks. The initial position of the domain is “remembered” for at least hundreds of generations.

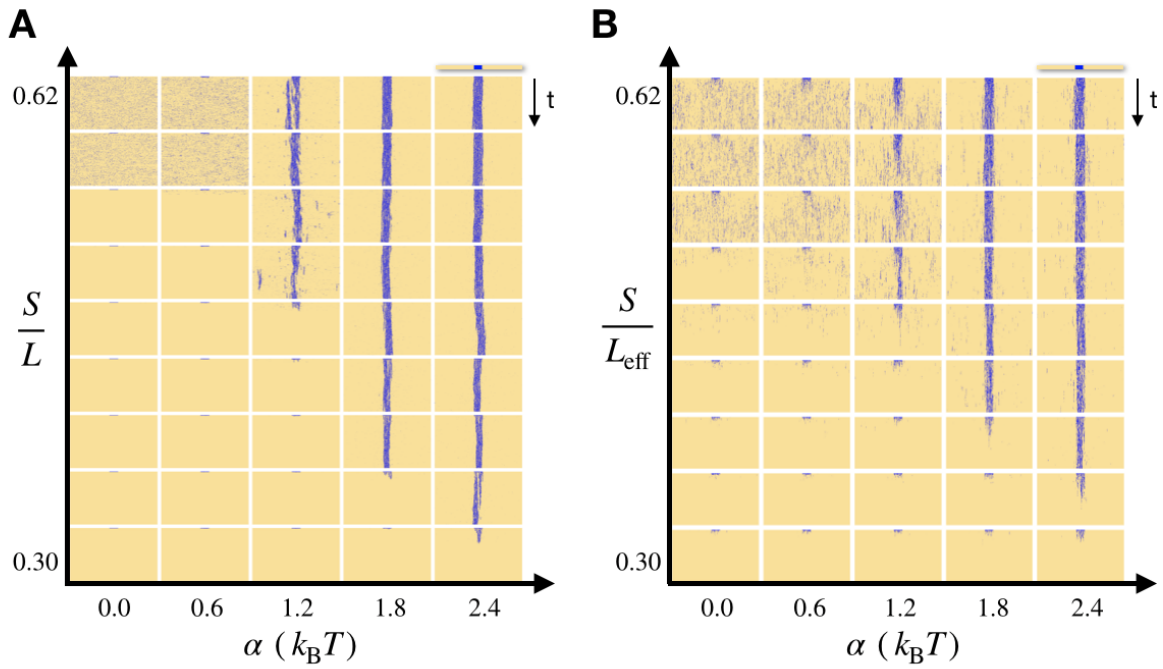


Fig. S2. Comparison of constant loss and replicative dilution. Comparison of the behavior of (A) our model with constant loss of marks at a rate L and (B) our model where loss is purely by dilution, periodically with period T_{div} . $L_{\text{eff}} = \log(2) / T_{\text{div}}$. In both panels, $E_T = 1000$.

5

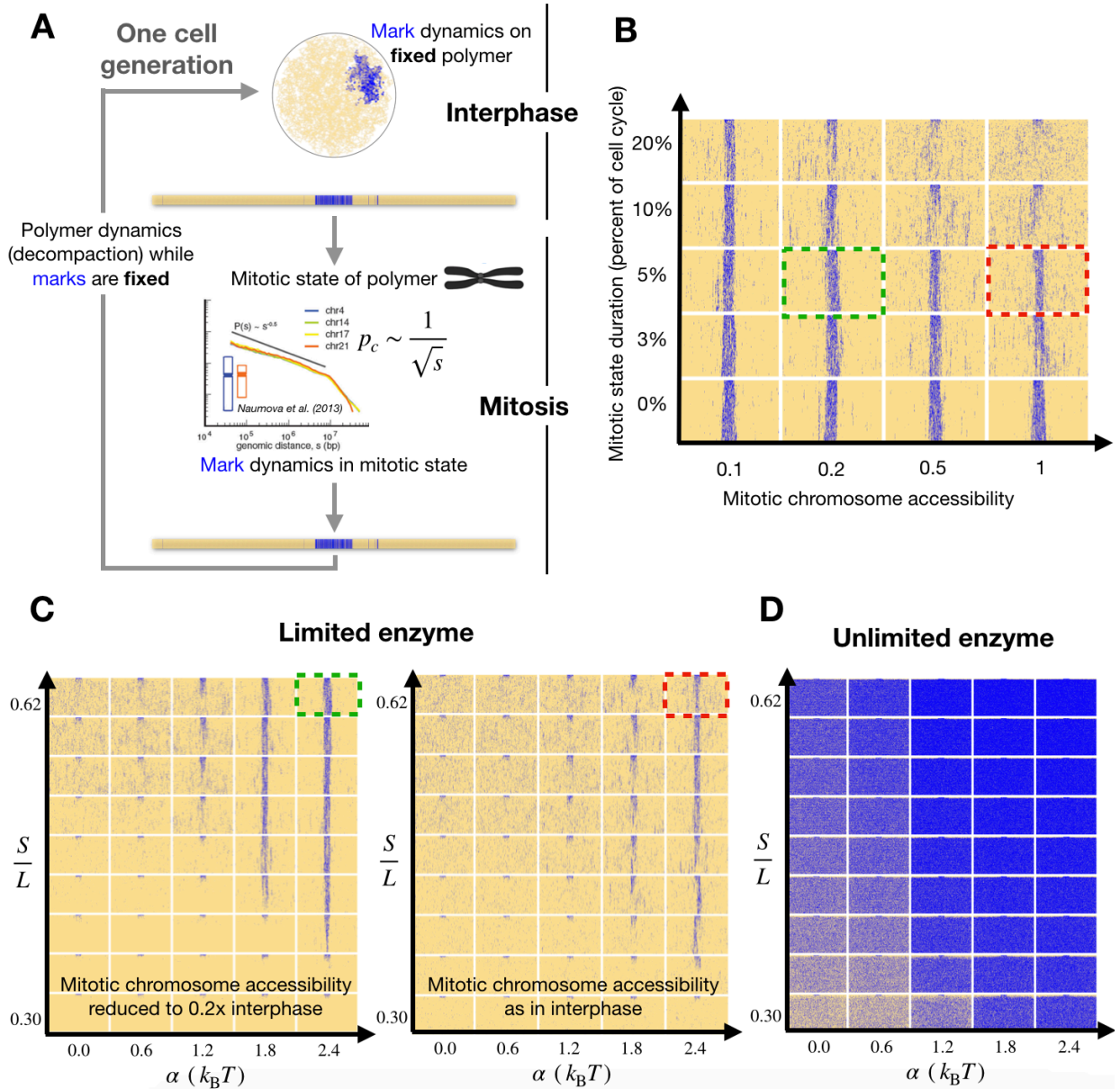


Fig. S3. Effects of mitotic spread of marks. (A) We elaborate our model of the cell cycle to include the possibility of marks spreading when chromatin is condensed during mitosis. We model the mitotic state using the $\sim 1/\sqrt{s}$ contact probability scaling from Hi-C experiments (92, 94). (B) Behavior of this model variant ($\alpha = 2.4$, $S/L = 0.62$, $E_T = 1000$, over 200 generations), for varying values of the mitotic duration and the accessibility of the mitotic chromosome to the enzyme. For a realistic mitotic duration of 5% of the cell cycle, memory is robust, regardless of whether accessibility is high (red frame) or low (green frame). (C) Behavior of this model variant (5% mitotic duration; $E_T = 1000$) for two different accessibility factors as α and S/L are varied, revealing little qualitative difference from the base model (c.f. Figure 3E). (D) Conditions identical to those of the right panel of (C), but with unlimited enzyme. Limited enzyme is essential for stability if there is mitotic spread.

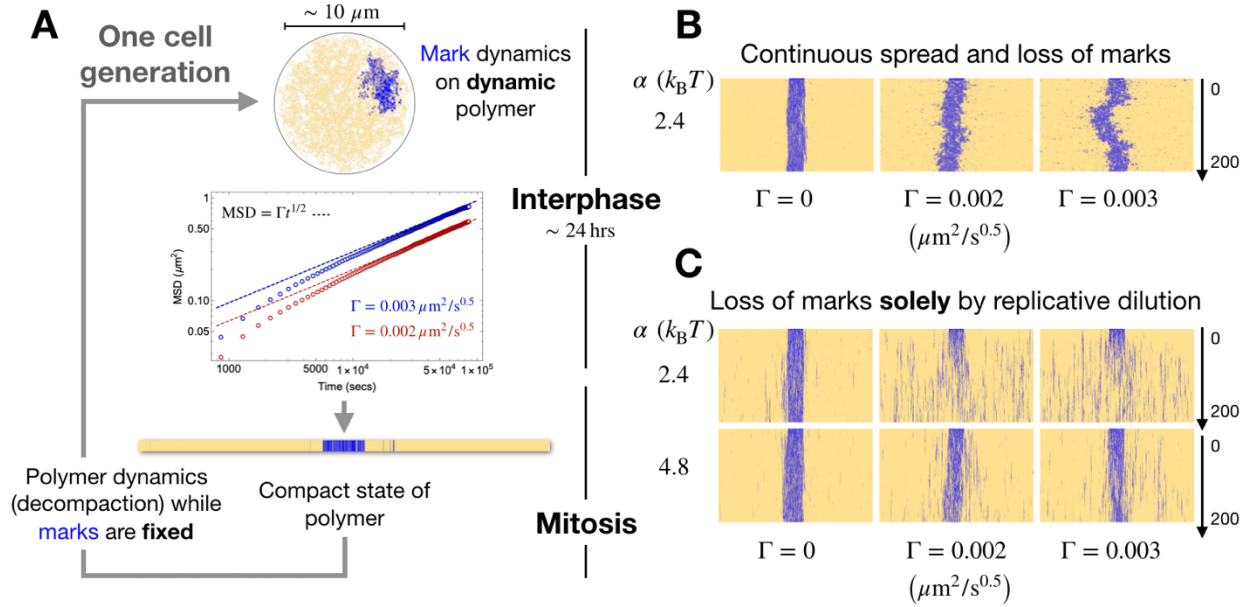


Fig. S4. Effects of interphase chromatin dynamics. (A) We elaborate our model of the cell cycle to include interphase chromatin dynamics. To set a realistic scale, we match our simulated dynamics to measured MSD scalings (32), assuming our confining sphere is 10 micrometers across and the duration of interphase is 24 hours. (B) The dynamics of our model ($\alpha = 2.4$, $S/L = 0.62$, $E_T = 1000$), with interphase dynamics of varying speeds, over 200 generations. (C) The dynamics of the dilution-only version of our model, with interphase dynamics of varying speeds and for two values of α , over 200 generations. Increasing α rescues the memory of mark domains.

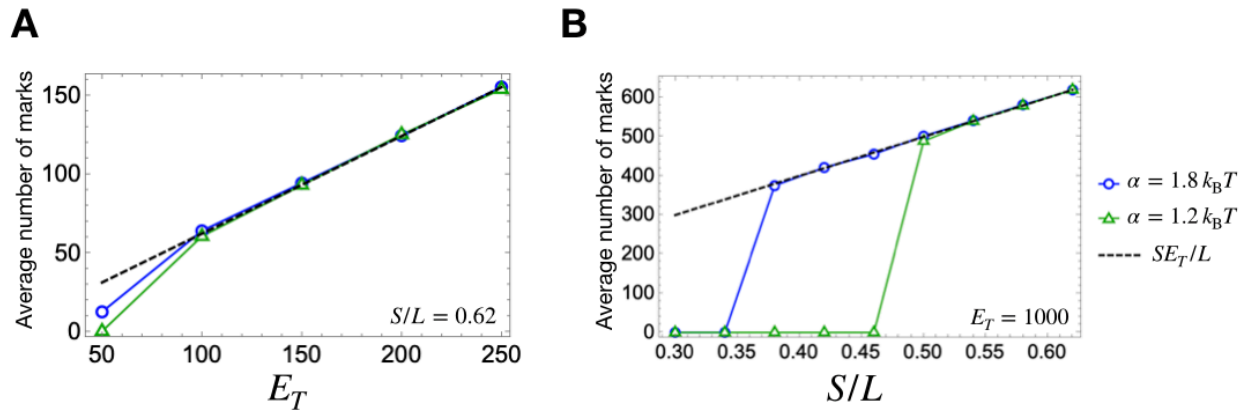
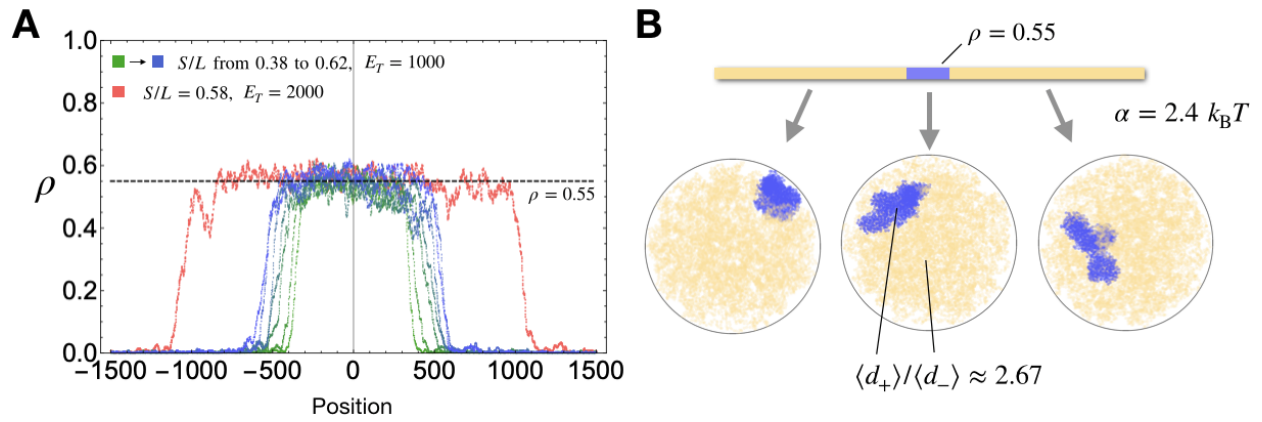


Fig. S5. Average number of marks as a function of E_T and S/L . In the limited enzyme model, as E_T (**A**) or S/L (**B**) are varied, the average number of marks is determined by the balance of spreading and loss to be SE_T/L (dashed line), whenever marks persist. As E_T is decreased (**A**), marks persist (in ever smaller regions) until there are so few they are vulnerable to stochastic extinction. By contrast (**B**), when S/L is decreased below its critical value (which depends on α), marks are lost suddenly and globally.

5

10



5 **Fig. S6. The character of semimarked domains. (A)** Centered profiles of stable domains arising in our model, averaged over many generations, showing that they are consistently *semimarked*—with a stable marking fraction of about $\rho = 0.55$. This marking fraction is insensitive to change in S/L or E_T . **(B)** Examples of the 3D shape of semimarked domains, illustrating their tendency to be aspherical.

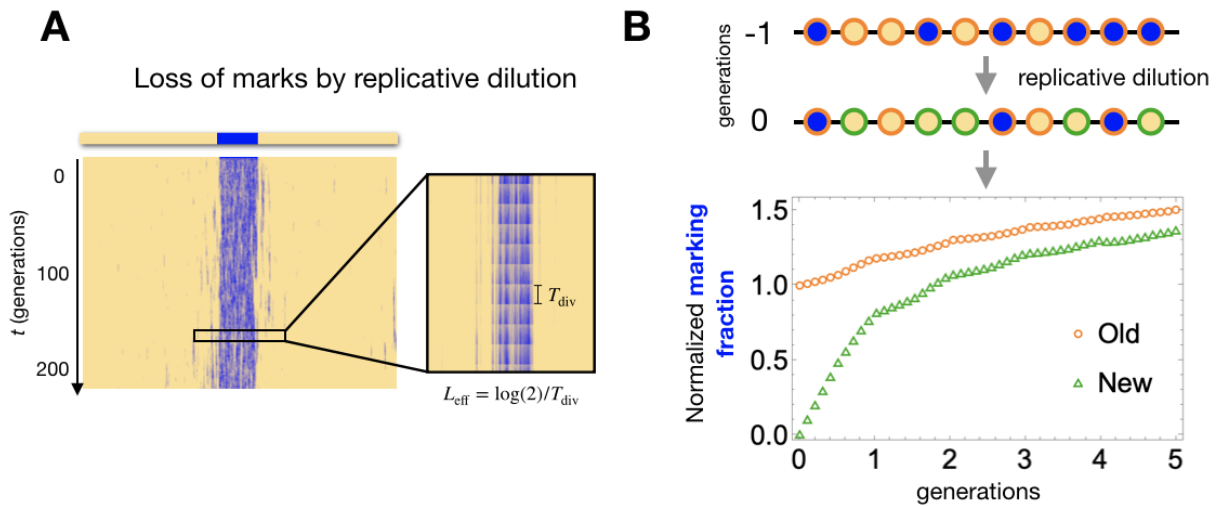


Fig. S7. Recovery of marks after replicative dilution. (A) In the variant of our model where loss is purely by replicative dilution ($\alpha = 2.4$, $S/L_{\text{eff}} = 0.50$, $E_T = 1000$), we keep track (B) of the marking fraction of the “new” monomers (green) that were replaced by dilution at a given time, losing their marks, and compare it to the marking fraction for the monomers that were not replaced (orange). The marking fraction (normalized to its value at the initial time) grows for both populations, a signature of semimarking. Compare e.g., to Figure 3, panel (e) of (37). Note when tracked over several generations, the old and new monomers accrue marks even though the average marking fraction across the domain is constant, because these two populations become an ever smaller fraction of the whole.

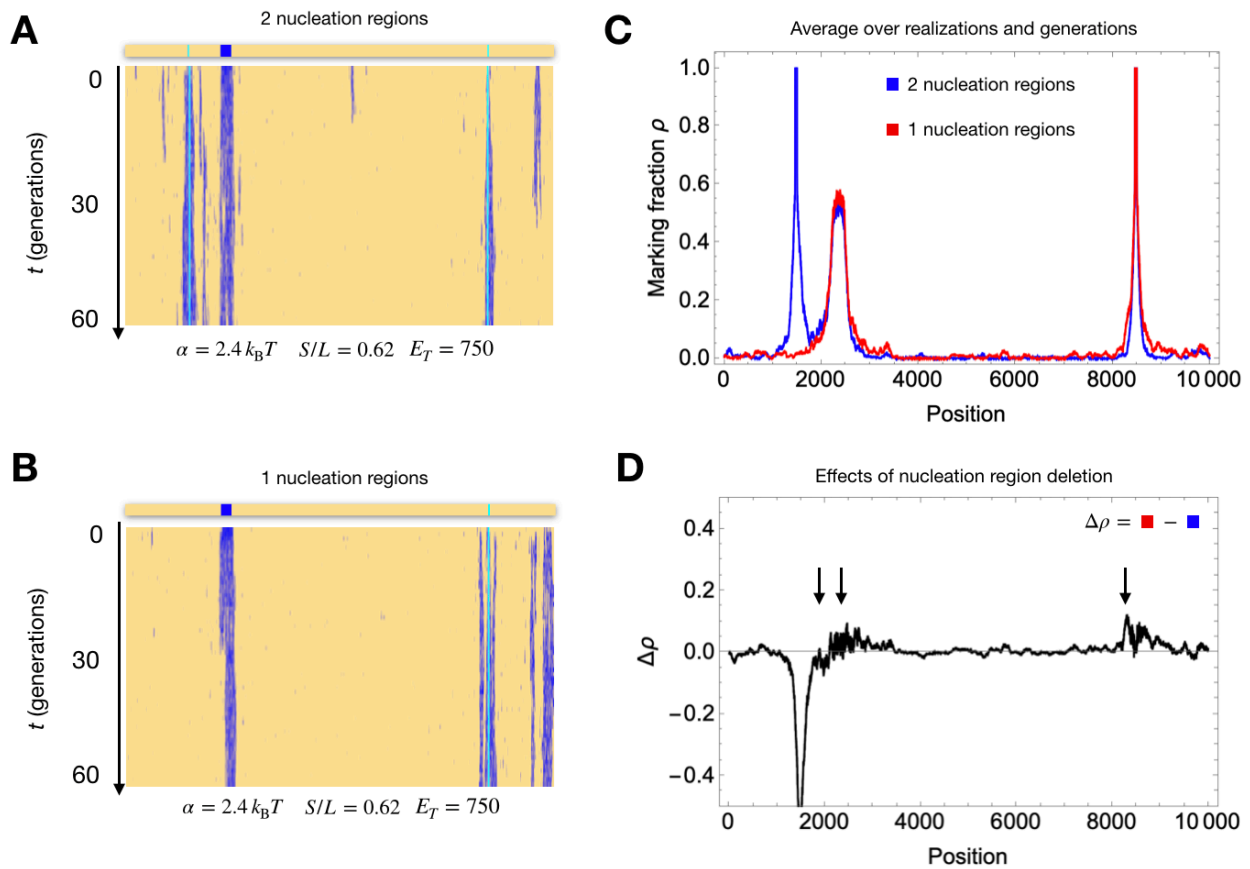


Fig. S8. Global mark redistribution due to deletion of a nucleation region. (A) Time evolution of a mark pattern consisting two nucleation regions (cyan; see Supplementary Text and Figure S11) and a separate initially marked domain. **(B)** Time evolution of the same initial pattern, with the left-hand nucleation region deleted. **(C)** The average marking fraction across the polymer, taken over many realizations of (A) (blue) and (B) (red) for 60 generations. **(D)** The difference in the average marking fraction caused by deletion of the nucleation region. We see local and distal changes (black arrows), including loss of marks near the deleted nucleation region and gain elsewhere. Compare to Fig. 3 of Kraft et al. (15).

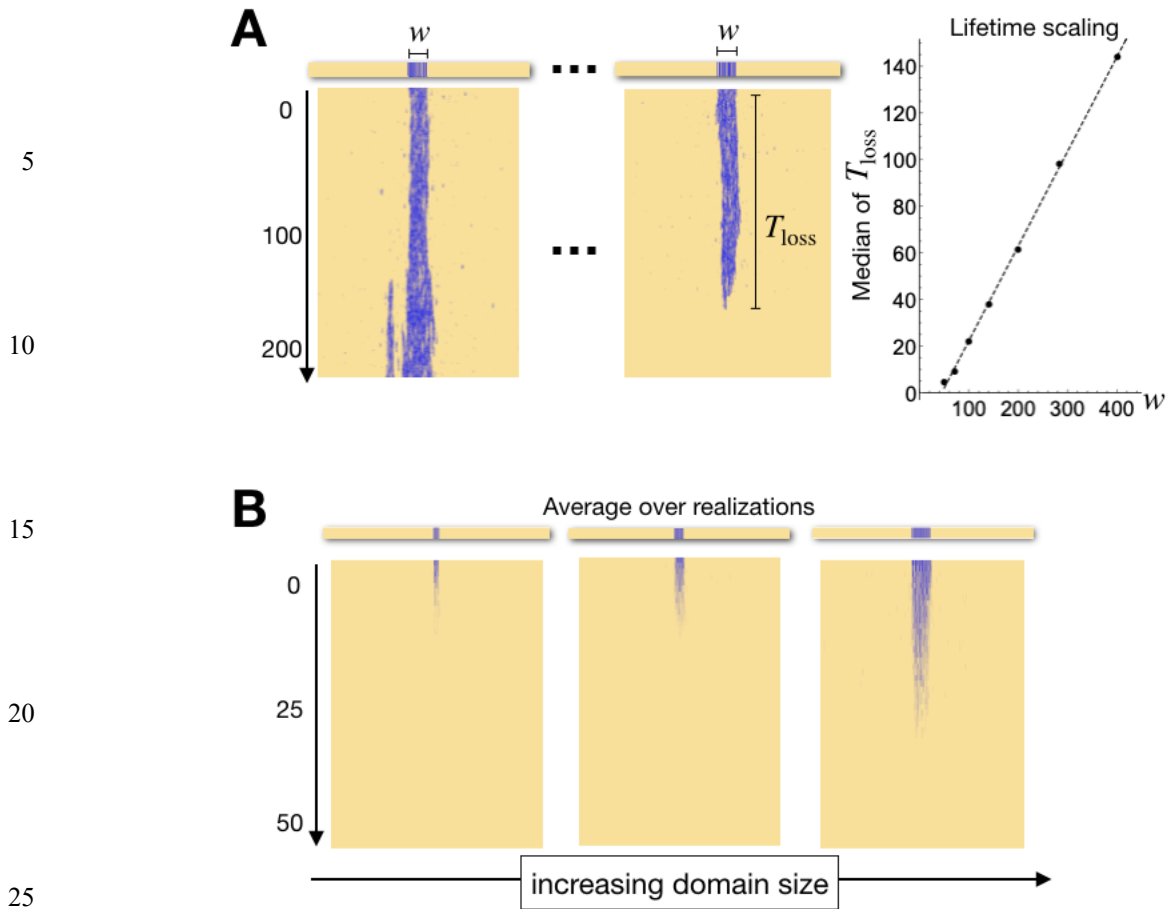


Fig. S9. Length dependence of mark redistribution. (A) Two equally-sized domains a long way apart compete for the limited enzyme pool ($\alpha = 2.4$, $S/L = 0.50$, $E_T = 2w$). Above a critical size, the time until one domain is lost by redistribution grows linearly with domain size. (B) A small domain competing with a much bigger one (not pictured) lasts longer, the bigger it is ($\alpha = 2.4$, $S/L = 0.50$; population average shown).

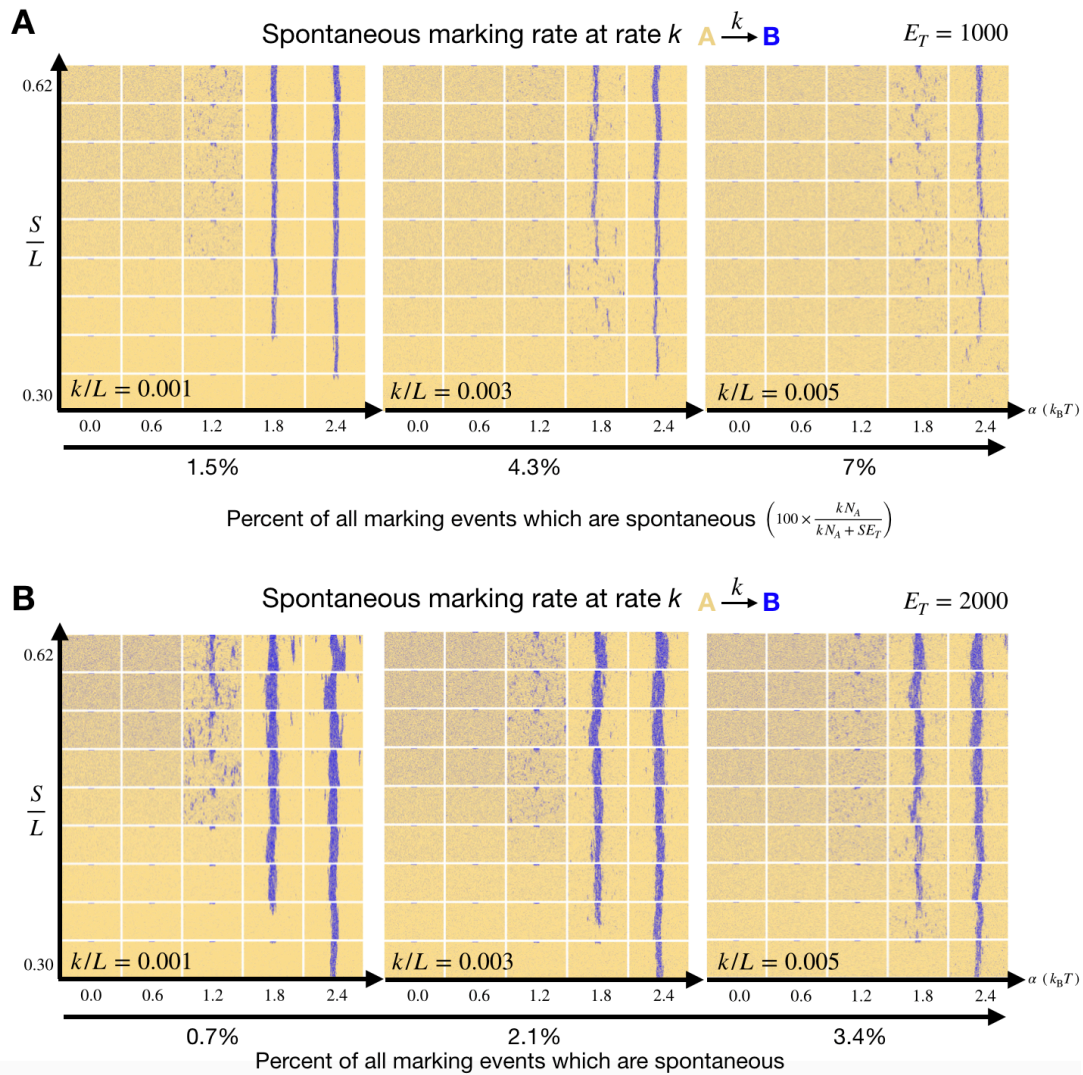


Fig. S10. Effects of spontaneous marking at a background rate. (A) The behavior of our model with the addition of spontaneous marking (A to B conversion) at a background rate k . We see a modest effect, unless a significant fraction of all marking events are spontaneous (e.g., $>7\%$, computed when $S/L = 0.62$). (B) As in (A) but with $E_T = 2000$.

5

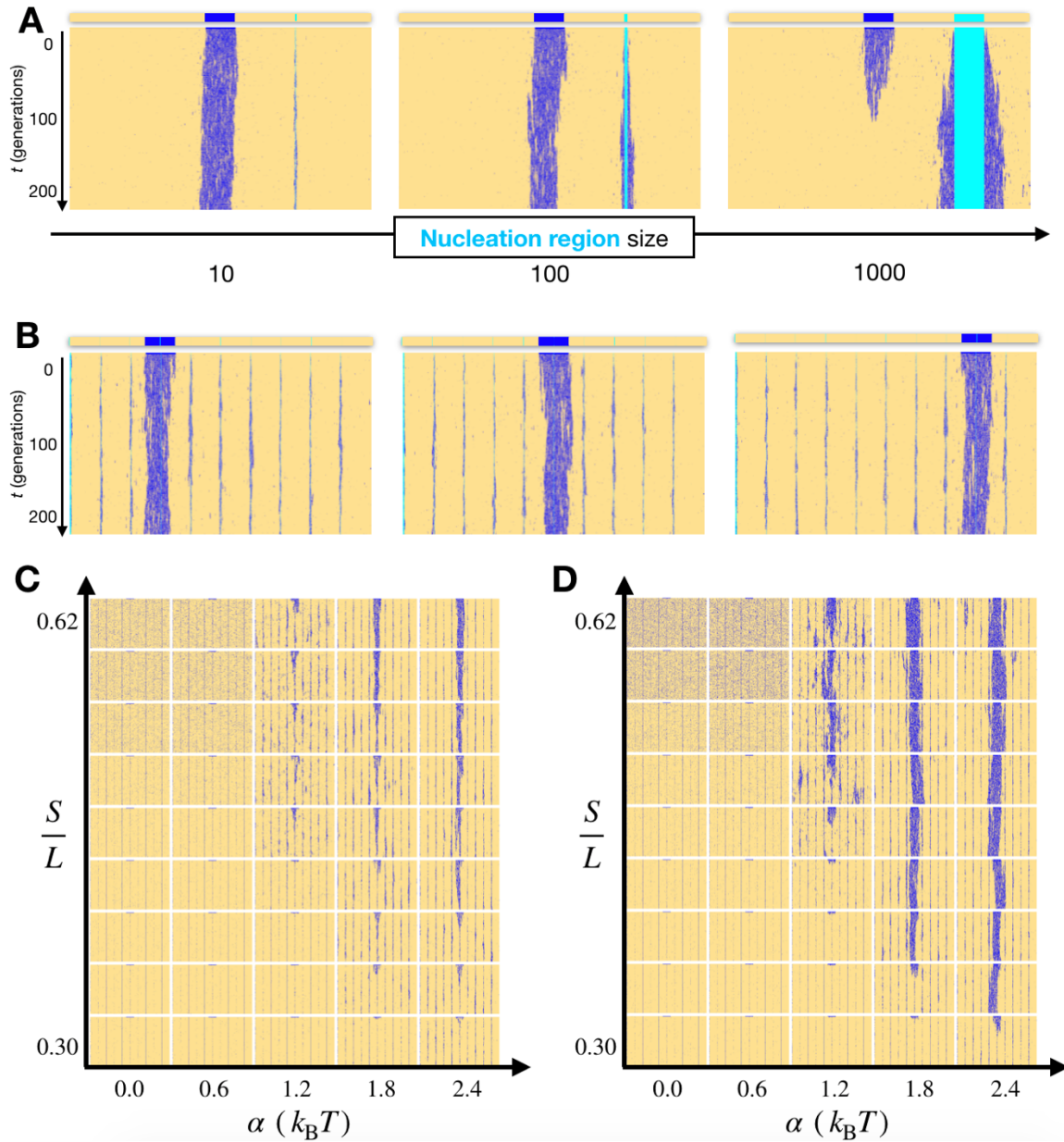


Fig. S11. Compatibility of our model with nucleation regions. (A) Time evolution of a single domain, as the size of a competing, adjacent nucleation region (cyan) is varied ($\alpha = 2.4$, $S/L = 0.62$, $E_T = 1000$). The domain remains stable except when the nucleation region is similar to the domain in size. (B) Memory of domain position is unaffected by an array of nucleation regions, each of size 10 monomers ($\alpha = 2.4$, $S/L = 0.62$, $E_T = 1000$). (C) Behavior of our model ($E_T = 1000$), with an array of nucleation regions (each of size 10 monomers), as α and S/L are varied. (D) As in (C), but with $E_T = 2000$.

5

10

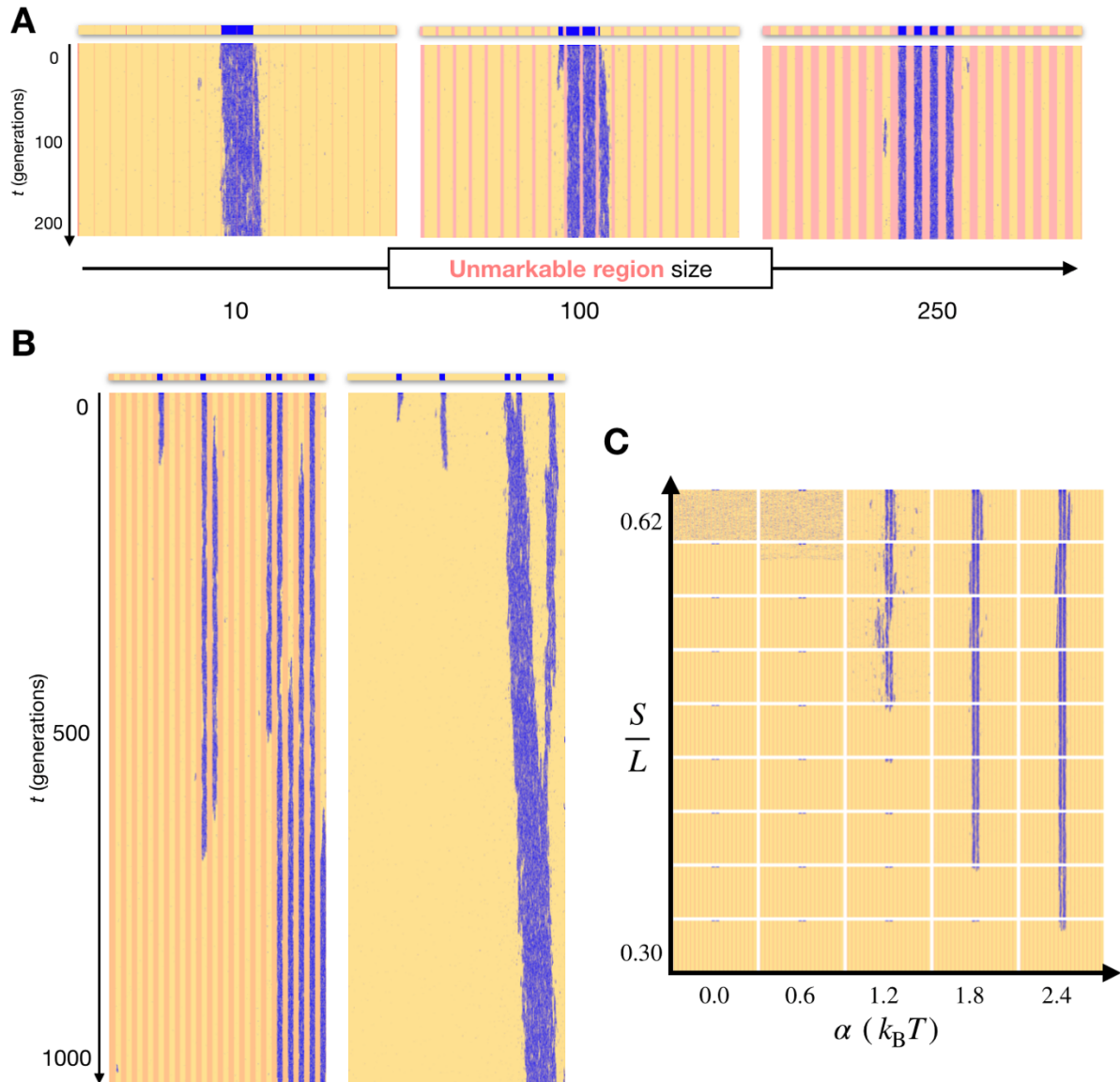


Fig. S12. Compatibility of our model with unmarkable regions. (A) Time evolution ($\alpha = 2.4$, $S/L = 0.62$, $E_T = 1000$) of an initial pattern consisting of a domain interrupted by an array of unmarkable regions (pink), as the width of the regions is varied. (B) Memory of a complex initial pattern with and without unmarkable regions ($\alpha = 2.4$, $S/L = 0.62$, $E_T = 1250$). Unmarkable regions appear to slow redistribution. (C) Behavior of our model ($E_T = 1000$), with an array of unmarkable regions of length 100 each, as S/L and α are varied.

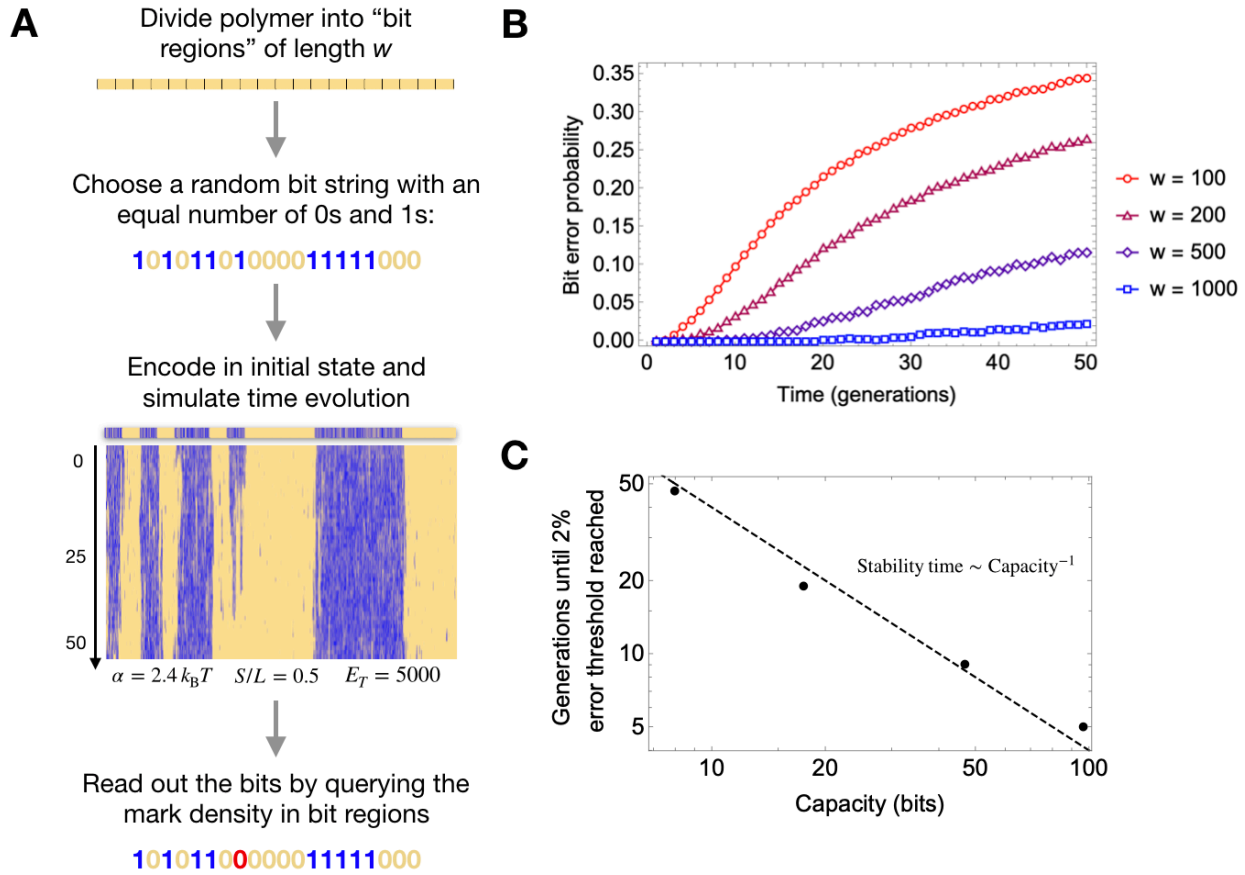


Fig. S13. Estimating the memory capacity of our model. (A) We introduce a scheme for encoding a string of bits into a mark pattern, and monitor its evolution over 50 generations. (B) The growth of the bit error probability (fraction of incorrect bits), for different values of the bit-width w . (C) The time in generations when the bit error probability reaches 0.02 as a function of the capacity in bits (see Supplementary Text for details), plotted on a log-log scale. We observe a roughly reciprocal relationship (dashed line for comparison).

5

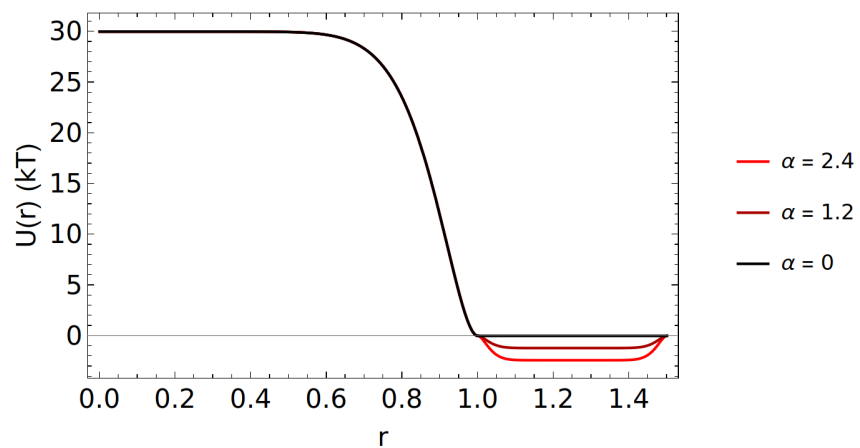


Fig. S14. Interparticle potential. The potential $U(r)$ we chose to govern interactions between monomers, for different values of the self-attraction parameter α .

5

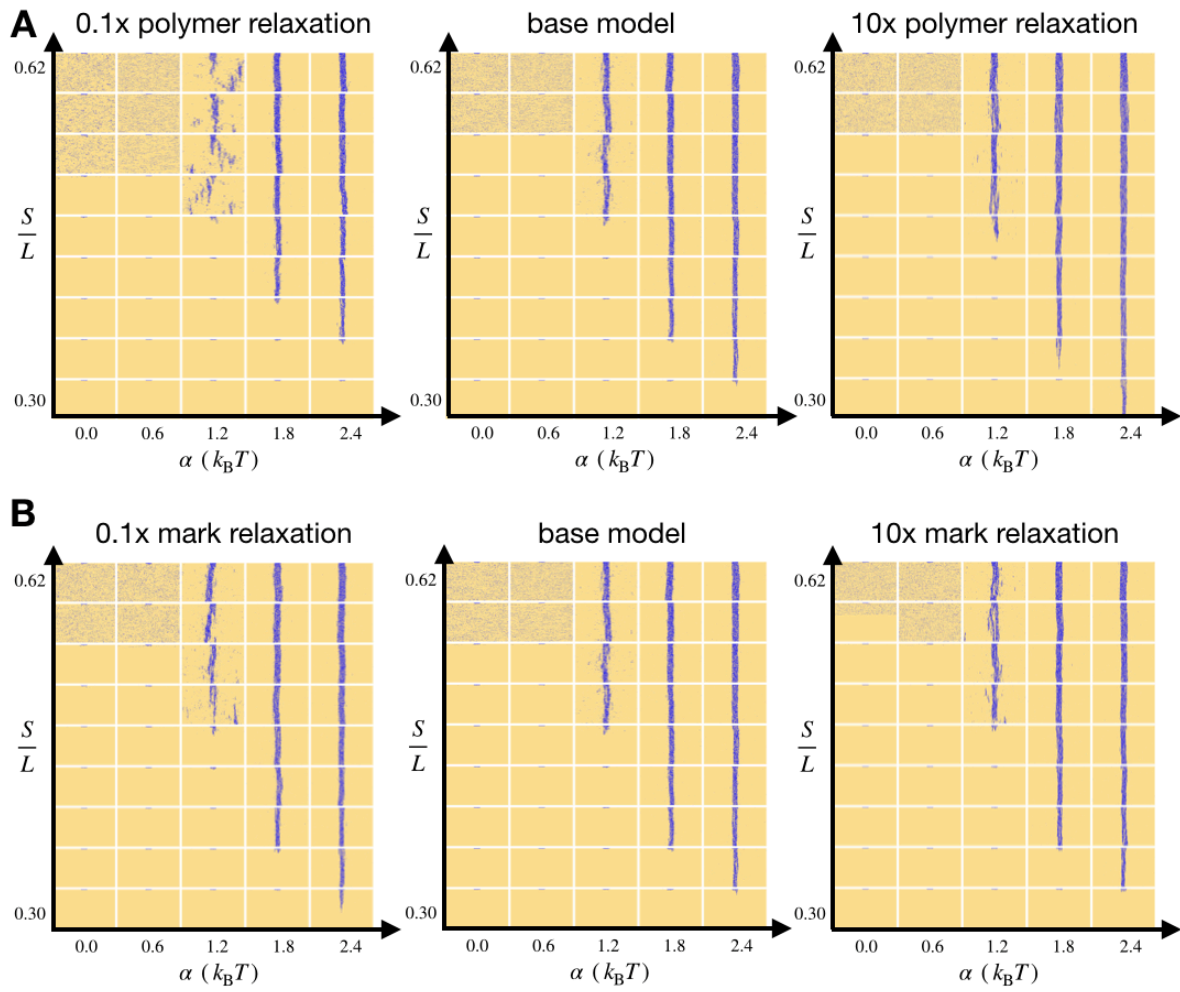


Fig. S15. Tests of relaxation. The behavior of our model as we vary the lengths of time that we relax the polymer (A) in “mitosis” or the marks (B) in interphase. $E_T = 1000$ in all panels.

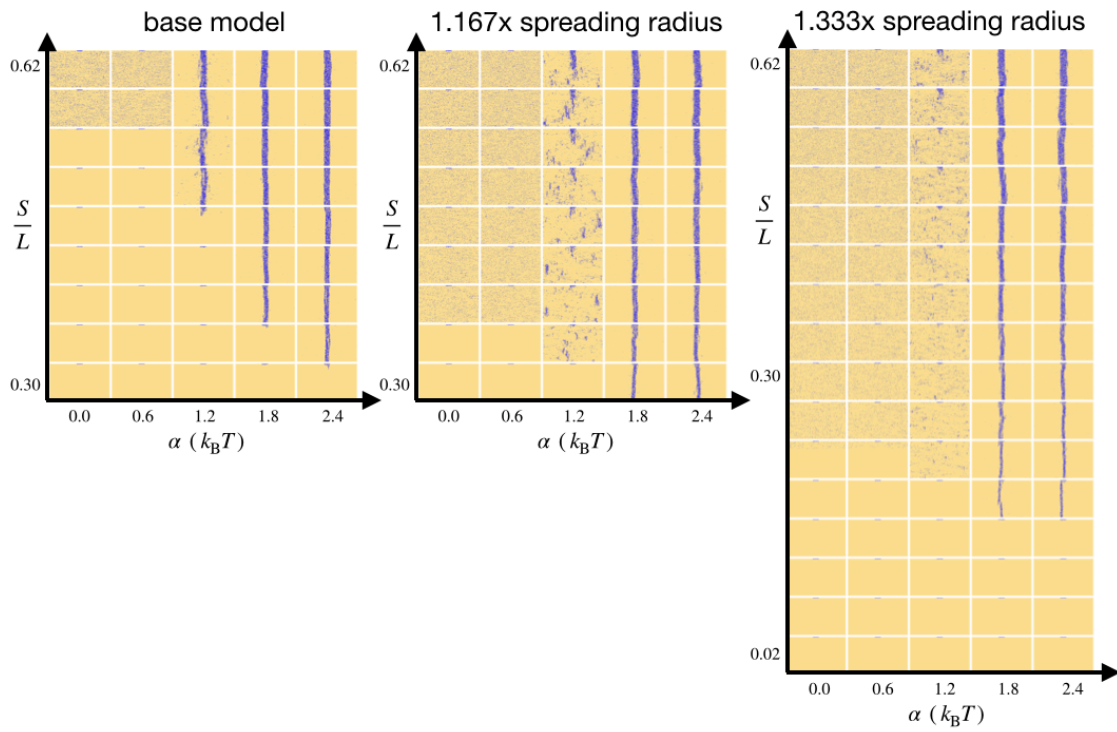


Fig. S16. Changing the spreading radius. The behavior of our model for different values of the mark spreading radius. The same qualitative behaviors are seen, though the parameter values where transitions occur (e.g., the critical values of S/L) change. $E_T = 1000$ in all panels.

5